

# TIDE: Two-Stage Inverse Degradation Estimation with Guided Prior Disentanglement for Underwater Image Restoration

Shravan Venkatraman<sup>1\*</sup> Rakesh Raj Madavan<sup>2\*</sup> Pavan Kumar S<sup>3\*</sup> Muthu Subash Kavitha<sup>4\*</sup>

<sup>1</sup>Mohamed bin Zayed University of AI <sup>2</sup>University of Amsterdam

<sup>3</sup>University of Massachusetts, Amherst <sup>4</sup>Nagasaki University

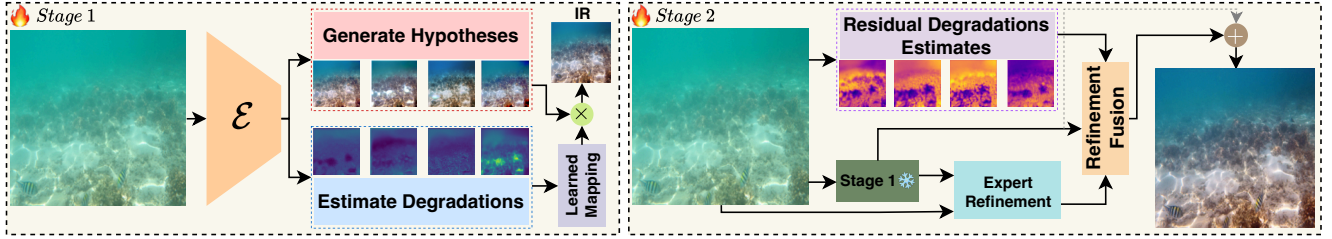


Figure 1. **Overview of the TIDE framework.** The pipeline consists of two stages. (1) Base restoration (left): The degraded image is processed by an encoder  $\mathcal{E}$ , producing features for degradation estimation and hypothesis generation. Multiple specialized restoration hypotheses are generated and fused based on estimated degradation maps via a learned mapping function. (2) Progressive refinement (right): The initial restoration and input image are analyzed to estimate residual degradations. Targeted corrections from refinement experts are selectively applied through a safety-gated fusion mechanism, yielding the final restored result.

## Abstract

Underwater image restoration is essential for marine applications ranging from ecological monitoring to archaeological surveys, but effectively addressing the complex and spatially varying nature of underwater degradations remains a challenge. Existing methods typically apply uniform restoration strategies across the entire image, struggling to handle multiple co-occurring degradations that vary spatially and with water conditions. We introduce *TIDE*, a two stage *inverse degradation estimation* framework that explicitly models degradation characteristics and applies targeted restoration through specialized prior decomposition. Our approach disentangles the restoration process into multiple specialized hypotheses that are adaptively fused based on local degradation patterns, followed by a progressive refinement stage that corrects residual artifacts. Specifically, *TIDE* decomposes underwater degradations into four key factors, namely color distortion, haze, detail loss, and noise, and designs restoration experts specialized for each. By generating specialized restoration hypotheses, *TIDE* balances competing degradation factors and produces natural results even in highly degraded regions. Extensive experiments across both standard benchmarks and challenging turbid water conditions show that

*TIDE* achieves competitive performance on reference based fidelity metrics while outperforming state of the art methods on non reference perceptual quality metrics, with strong improvements in color correction and contrast enhancement. Our code is available at: <https://rakesh-123-cryp.github.io/TIDE/>.

## 1. Introduction

Underwater image restoration (UIR) is a critical problem in computer vision with applications in marine biology, archaeology, robotics, and ocean engineering. Underwater images suffer from wavelength-dependent color distortion, low contrast, haze from scattering, blurriness, and noise, which degrade both visual quality and downstream tasks such as detection and scene understanding. Deep learning methods, including generative approaches [8, 22], zero-shot methods [16, 29, 49], and medium-guided strategies [21], have advanced the field, yet they struggle with the complex, spatially varying nature of underwater degradations. A single image may simultaneously contain regions with different types and severities of distortions due to variations in depth, lighting, and water properties. However, existing methods implicitly assume a generic and homogeneous degradation distribution across images in a dataset, overlooking this inherent spatial and contextual

\*Equal contribution.

variability. As a result, they often deliver suboptimal outcomes: when tuned for severely degraded regions, they over-process well-preserved areas and introduce artifacts; when calibrated conservatively, they leave challenging regions under-restored.

Recent approaches have attempted to address spatially varying degradations in underwater imagery. Multi-scale architectures [9, 28, 32, 42] extract features at different resolutions to capture degradations of varying scales. Attention-based methods [32, 45, 51, 57] dynamically weight features based on their importance for restoration. Some approaches [23, 41, 46, 55] employ dual-branch networks that separately handle color correction and dehazing before fusion. Graph-based methods [19, 50] model relationships between different image regions to adapt restoration parameters locally. While these approaches improve upon uniform processing, they typically generate a single restoration output directly and lack explicit mechanisms to handle the co-occurrence of multiple degradation types in different regions. Additionally, they often struggle with error accumulation, where inaccuracies in initial processing stages propagate to the final output without corrections.

To this end, we introduce TIDE, a framework for UIR through explicit degradation modeling and progressive refinement. TIDE implements two key innovations: (1) inverse degradation mapping with specialized prior decomposition, which disentangles different degradation types and applies targeted restoration strategies; and (2) two-stage degradation compensation, which identifies and corrects residual degradations after initial restoration. In the first stage, TIDE estimates pixel-wise degradation maps for color distortion, contrast reduction, detail loss, and noise. Then it generates specialized restoration hypotheses using decoders designed with inductive biases for each type of degradation. These hypotheses are dynamically fused based on the estimated degradation maps, producing a spatially varying restoration that addresses each region’s specific degradation characteristics. Despite this targeted approach, severely degraded regions (e.g., turbid water or low-light areas) may retain residual artifacts after the first stage. Our second stage explicitly analyzes these residual degradations, generating targeted correction terms through focused refinement experts, and applying these corrections selectively to regions requiring further enhancement.

Figure 1 illustrates the TIDE framework architecture. The base model first extracts multi-scale features from the degraded input image. These features serve two parallel paths: (1) degradation estimation, which produces pixel-wise maps indicating the spatial distribution and severity of different degradation types, and (2) hypothesis generation, where specialized decoders generate restoration candidates targeting specific degradation types. Each decoder embeds domain-specific inductive biases, and a learned map-

ping function adaptively fuses these hypotheses based on the degradation maps, producing an initial restoration. The second stage focuses on residual degradations by contrasting the input with the initial restoration. This differential signal steers refinement experts that predict targeted corrections, which are then fused through a gated mechanism to enhance only the degraded regions while preserving well-restored areas. Such progressive refinement lets TIDE handle complex, non-uniform degradations more effectively than single-stage methods, as seen in Figure 1.

To summarize, our main contributions are:

- We present TIDE, a framework that addresses complex, spatially varying underwater degradations through a structured, multi-stage restoration process.
- We introduce a degradation-specific hypothesis generation and fusion strategy, which produces targeted corrections for distinct degradation types and combines them adaptively to handle heterogeneous distortions.
- We develop a residual-aware refinement mechanism that selectively enhances poorly restored regions, improving overall fidelity and perceptual quality without compromising well-recovered areas.

## 2. Related Works

**Underwater Image Restoration.** UIR typically relied on traditional image processing techniques such as histogram equalization, white balance correction, and physics-based dehazing methods [6, 10, 17]. While these methods improve visual contrast and partially correct color distortions, they often struggle to generalize across diverse underwater scenes and miss fine image details. Deep learning solutions have achieved significant improvements [13, 18, 20, 21, 35, 43, 44, 48]. GANs, in particular, enable realistic dataset synthesis and unpaired image enhancement [11, 12, 26]. Ucolor addresses color distortion and poor contrast using a multi-color space encoder with attention [21], FUSION leverages spatial and frequency domain information for effective fusion and color recalibration [45], and FUNIE-GAN and Water-Net restore color fidelity and perceptual realism via adversarial optimization and confidence-guided fusion [24, 54].

**Multi-Hypothesis and Progressive Image Recovery.** Progressive architectures and multi-hypothesis strategies, such as recursive residual networks and staged refinement modules, have proven effective for complex image restoration by simplifying optimization and improving accuracy [36, 52]. Recent work extends this by explicitly modeling degradation or domain characteristics, e.g., ingredient-aware reformulations [53], severity-aware weather removal [5], and multi-weather restoration via domain translation [30]. In the super-resolution domain, multi-hypothesis techniques have been used to fuse spa-

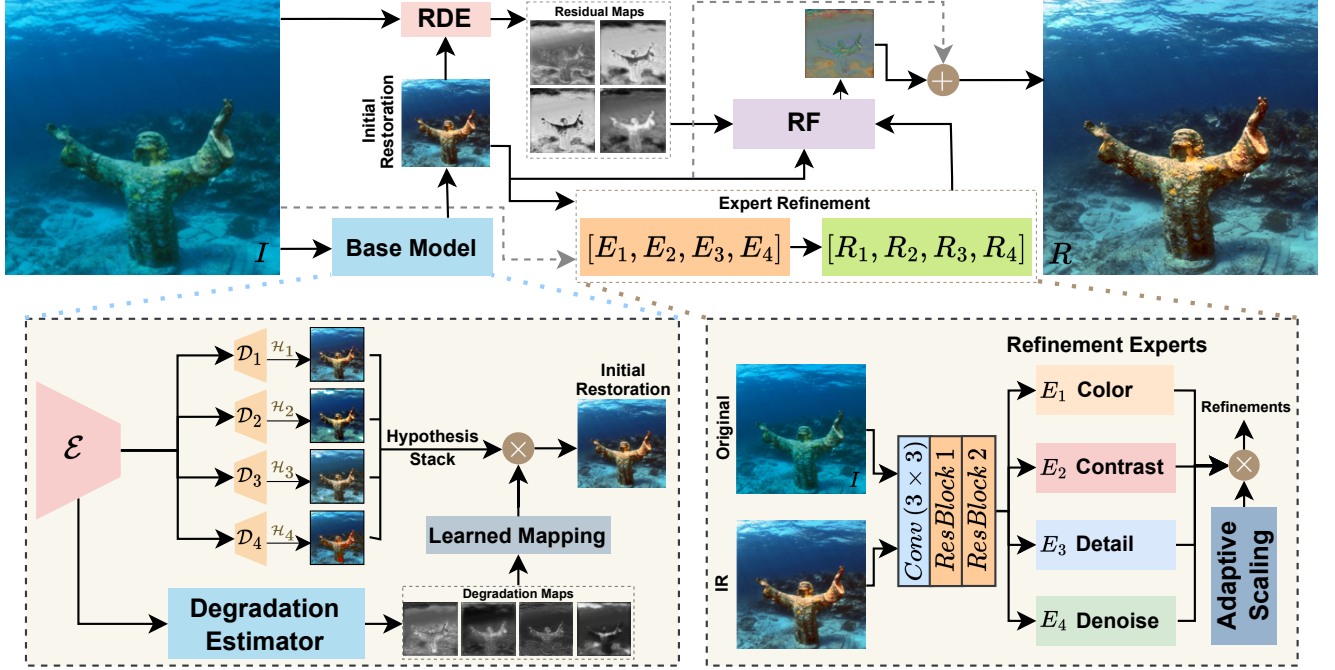


Figure 2. **Architecture of the TIDE framework.** The top shows the overall flow: the input image is first processed by the base model to generate an initial restoration, which along with the original image feeds into the residual degradation estimator (RDE) and refinement fusion (RF) to produce the final output. The bottom left shows the base model details, where a feature extractor  $\mathcal{E}$  feeds specialized decoders  $\mathcal{D}_1$ - $\mathcal{D}_4$  that generate restoration hypotheses  $\mathcal{H}_1$ - $\mathcal{H}_4$ , while also estimating degradation maps. These hypotheses are combined through a learned mapping function for initial restoration. The bottom right illustrates the refinement stage, where the original and initially restored images are processed by shared convolutional processing before being fed to specialized refinement experts  $E_1$ - $E_4$  that generate targeted corrections for color, contrast, detail, and noise, which are then adaptively scaled and combined.

tially offset patches and improve restoration of compressed screen content [47]. Other approaches combine progressive designs with semantic priors or reference images to tackle specific tasks, such as face restoration through semantic-aware style transfer [3], reference-guided multi-degradation refinement [56], and staged fusion for HDR reconstruction with attention [4]. Task-specific systems like PRISM progressively reconstruct scene graph image edits [15], while lensless image restoration frameworks integrate multi-stage supervision with GAN refinement [25].

### 3. Method

#### 3.1. Overview

We approach UIR via inverse degradation estimation and prior disentanglement. Instead of directly mapping degraded images  $\mathbf{I}$  to clean ones, we explicitly model degradations and apply targeted restoration. The process is formulated as  $\hat{\mathbf{J}} = \mathcal{R}(\mathbf{I}, \mathcal{D}(\mathbf{I}))$ , where  $\hat{\mathbf{J}}$  is the restored image,  $\mathcal{R}$  is the restoration function, and  $\mathcal{D}$  estimates degradation maps  $\mathbf{M} = \{M_1, \dots, M_K\}$  for  $K$  degradation types.

Different degradations require specialized treatment. Through prior disentanglement, we generate multiple hy-

potheses  $\mathbf{H} = \{H_1, \dots, H_K\}$ , each addressing a specific degradation via  $H_i = \mathcal{F}_i(\mathbf{I})$ , where  $\mathcal{F}_i$  is the corresponding specialized function. TIDE implements this in two stages: first, degradation-guided multi-hypothesis restoration combines specialized hypotheses (§ 3.2); second, a refinement stage corrects residual degradations (§ 3.3). Fig. 2 illustrates the architecture with its targeted components and progressive refinement.

#### 3.2. Inverse Degradation Mapping with Specialized Prior Decomposition

The first stage of TIDE performs inverse degradation mapping to identify the spatial distribution and severity of different degradation types, followed by specialized prior decomposition to generate targeted restoration hypotheses.

**Degradation Estimation.** To restore underwater images effectively, we first identify the degradations affecting each spatial location. We design a lightweight encoder-decoder network  $\mathcal{D}$  that maps an input image  $\mathbf{I} \in \mathbb{R}^{3 \times H \times W}$  to  $K$  degradation maps  $\mathbf{M} = \mathcal{D}(\mathbf{I}) \in \mathbb{R}^{K \times H \times W}$ , where each element  $M_k(x, y) \in [0, 1]$  indicates the severity of degradation type  $k$  at spatial location  $(x, y)$ . The network uses a multi-scale architecture with skip connections to capture



both local and global patterns. It consists of an initial feature extraction layer  $f_0$ , a series of downsampling layers  $\{f_d^i\}_{i=1}^N$ , a global context module  $f_g$ , and upsampling layers  $\{f_u^i\}_{i=1}^N$  with skip connections. The global context module aggregates spatial information via global average pooling followed by channel-wise modulation. The output degradation maps are generated through a sigmoid activation,  $\mathbf{M} = \sigma(W_o f_u^1(f_u^2(\dots f_u^N(\mathbf{g}, \mathbf{z}_{N-1}) \dots), \mathbf{z}_0))$ , where  $W_o$  is the output projection and  $f_u^i(\mathbf{a}, \mathbf{b})$  denotes the  $i$ -th up-sampling layer with skip connection from feature map  $\mathbf{b}$ .

**Inverse Degradation Mapping with Specialized Prior Decomposition.** We decompose underwater image degradation into four fundamental types - color distortion, contrast reduction, detail loss, and noise - motivated by the underlying imaging physics [1, 7, 14]. Color distortion arises from wavelength-dependent attenuation, where longer wavelengths (red) diminish faster than shorter ones (blue/green) [2]. The reduction in contrast occurs due to the scattering of light by suspended particles, which produces haze and reduces the dynamic range [37]. Detail loss results from absorption and forward scattering that blur fine structures [34], while noise originates from sensor limitations in low-light conditions and scattering effects such as marine snow [40]. While other degradation types such as extreme low-light or turbidity-related scatter could be considered, our experiments show these are effectively captured by the existing experts: low-light effects manifest primarily as contrast reduction and increased noise, and turbidity-related scatter is captured by the noise decoder. Our ablations (Table 2) justify that these four types of degradation form a minimal but sufficient set for effective restoration, balancing restoration quality with computational efficiency while avoiding unnecessary complexity.

**Specialized Restoration Decoders.** We design  $K = 4$  specialized decoders, each targeting one degradation type: color distortion, contrast reduction, detail loss, and noise. All decoders share a common feature extraction backbone  $\mathcal{E}$ , which generates hierarchical representations  $\mathbf{F} = \{\mathbf{f}_0, \mathbf{f}_1, \dots, \mathbf{f}_N\}$  from the input image  $\mathbf{I}$ , i.e.,  $\mathbf{F} = \mathcal{E}(\mathbf{I})$ . Each specialized decoder produces a restoration hypothesis  $H_k = \mathcal{F}_k(\mathbf{F})$  for  $k \in \{1, 2, 3, 4\}$ , with architectural inductive biases that guide them toward their target degradation.

The color restoration decoder  $\mathcal{F}_1$  uses channel-wise attention ( $\mathbb{R}^C \rightarrow \mathbb{R}^{C/r} \rightarrow \mathbb{R}^C$ ) to correct wavelength-dependent attenuation. The contrast enhancement decoder  $\mathcal{F}_2$  employs residual blocks  $\phi : \mathbb{R}^{C \times H \times W} \rightarrow \mathbb{R}^{C \times H \times W}$  to address scattering-induced contrast loss. The detail recovery decoder  $\mathcal{F}_3$  implements cascaded residual blocks with cumulative enhancement  $\mathcal{E}_d(\mathbf{x}) = \mathbf{x} + \sum_{i=1}^L \mathcal{R}_i(\mathbf{x})$  to recover fine structures lost through medium absorption. The denoising decoder  $\mathcal{F}_4$  applies group convolutions with  $g = \min(\lfloor C/8 \rfloor, C)$  partitions to remove noise from sus-

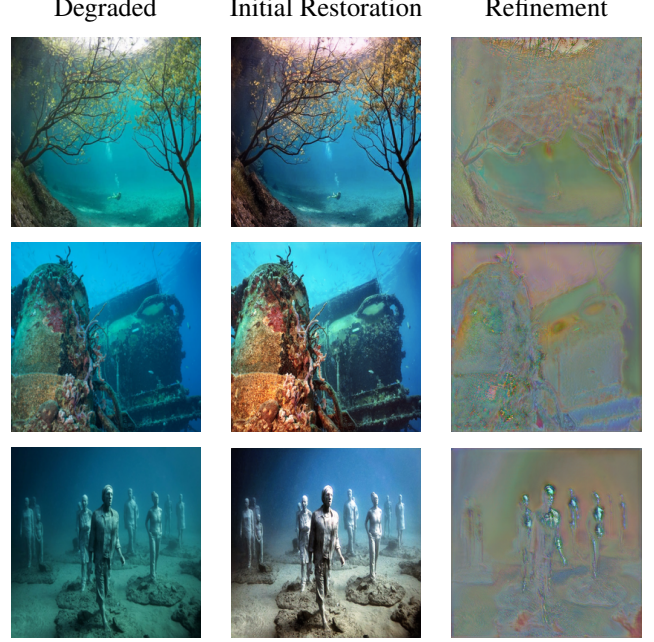


Figure 3. Visual comparison of input degradations, initial restoration, and expert refinement stages, illustrating TIDE’s progressive restoration process.

pended particles.

This specialization is reinforced during training via two losses. The diversity loss  $\mathcal{L}_{div}(\mathbf{H}) = \frac{1}{N_{pairs}} \sum_{i=1}^K \sum_{j=i+1}^K \cos\_sim(H_i, H_j)$  regularizes similarity between hypotheses, preventing redundant representations, and the degradation consistency loss  $\mathcal{L}_{dc}(\mathbf{M}, \mathbf{I}, \mathbf{J}) = \mathcal{L}_{MSE}(\sum_{k=1}^K M_k, \text{norm}(|\mathbf{I} - \mathbf{J}|))$  aligns estimated degradation maps with actual degradation patterns. Together, these losses allow each decoder to develop optimal strategies for its target degradation without requiring explicit labels, enabling the system to handle complex, co-occurring degradations effectively.

**Adaptive Fusion Mechanism.** Given the  $K$  specialized restoration hypotheses  $\{H_1, H_2, \dots, H_K\}$  and the degradation maps  $\mathbf{M}$ , we perform an adaptive fusion to combine them into the final restored image. The fusion process generates pixel-wise weights  $\mathbf{W} \in \mathbb{R}^{K \times H \times W}$  that determine the contribution of each hypothesis at each spatial location:

$$\hat{\mathbf{J}}_1 = \sum_{k=1}^K W_k \odot H_k \quad (1)$$

where  $W_k$  is the weight map for hypothesis  $H_k$ , and  $\odot$  represents element-wise multiplication. We implement three fusion strategies, with the learned fusion being our primary approach. The learned fusion mechanism transforms degradation maps into fusion weights through a non-linear



mapping. This enables the model to select the appropriate restoration strategy for each image region based on its specific degradation characteristics.

### 3.3. Two-Stage Degradation Compensation with Expert-Guided Correction

Our second stage implements a progressive refinement approach that explicitly identifies and addresses these remaining artifacts through differential degradation analysis and expert-guided correction.

**Differential Degradation Analysis.** Residual degradations are identified by estimating discrepancies between the initial restoration  $\hat{\mathbf{J}}_1$  and the degraded input  $\mathbf{I}$ . We implement this through a differential degradation analysis function  $\mathcal{D}_2$ , which predicts spatial residuals:  $\mathbf{M}_r = \mathcal{D}_2(\mathbf{I}, \hat{\mathbf{J}}_1)$ , where  $\mathbf{M}_r \in \mathbb{R}^{K \times H \times W}$  represents the residual degradation maps for the  $K$  degradation types. First, it computes an absolute difference map  $\mathbf{D} = |\mathbf{I} - \hat{\mathbf{J}}_1|$  to localize regions with remaining degradations. Since not all discrepancies indicate incomplete restoration, we process the concatenated input  $[\mathbf{I}, \hat{\mathbf{J}}_1] \in \mathbb{R}^{6 \times H \times W}$  through an attention network guided by  $\mathbf{D}$ :

$$\mathbf{M}_r = \sigma(f_r([\mathbf{I}, \hat{\mathbf{J}}_1]) \cdot (1 + \alpha \cdot f_d(\mathbf{D}))) \quad (2)$$

where  $f_r$  is the residual estimation network,  $f_d$  is the difference enhancement network,  $\alpha$  is a learnable scaling factor, and  $\sigma$  is the sigmoid function. This allows the network to focus on regions with significant residual degradations while considering contextual information from both the input and initial restoration.

**Expert-Guided Correction Generation.** Based on the residual degradation maps, we generate targeted corrections for each degradation type using specialized refinement experts. Each expert  $\mathcal{E}_k$  takes the original image and initial restoration as inputs and produces a correction term  $C_k = \mathcal{E}_k(\mathbf{I}, \hat{\mathbf{J}}_1)$ ,  $k \in \{1, 2, 3, 4\}$ , specific to its degradation type. We design four refinement experts corresponding to the same degradation types addressed in the first stage. Each expert implements specialized processing tailored to its target degradation, generating a correction term rather than a complete restoration. To prevent excessive corrections that might introduce artifacts, each expert includes an adaptive scaling mechanism  $C_k = \tanh(f_k(\mathbf{I}, \hat{\mathbf{J}}_1)) \cdot \sigma(s_k)$ , where  $f_k$  denotes the expert’s processing function,  $\tanh$  constrains the correction range to  $[-1, 1]$ , and  $s_k$  is a learnable scaling parameter controlling the correction magnitude.

**Safety-Gated Fusion.** The correction terms from individual experts are then carefully combined to avoid over-correction. We implement a safety-gated fusion mechanism that considers both the residual degradation maps and the quality of the initial restoration:

$$\mathbf{C} = \left( \sum_{k=1}^K (M_r)_k \odot C_k \right) \cdot G(\hat{\mathbf{J}}_1) \cdot \sigma(s_g) \quad (3)$$

where  $(M_r)_k$  is the residual map for degradation type  $k$ ,  $G$  is a safety gate function that limits corrections in well-restored regions, and  $s_g$  is a global scaling factor. The safety gate  $G$  examines the initial restoration  $\hat{\mathbf{J}}_1$  and produces a spatial mask that modulates the correction intensity, computed as  $G(\hat{\mathbf{J}}_1) = \sigma(f_g(\hat{\mathbf{J}}_1))$ , where  $f_g$  consists of convolutional layers that identify regions requiring minimal correction. The final restoration is then obtained by adding the fused correction map  $\mathbf{C}$  to the initial restoration as  $\hat{\mathbf{J}} = \hat{\mathbf{J}}_1 + \mathbf{C}$ , followed by a clamping operation to ensure that the pixel values remain within the valid range  $[0, 1]$ .

**Optimization.** We train our two-stage framework with a structured two-phase optimization. In stage 1, we optimize only the base model with reconstruction, diversity, and degradation-consistency losses:  $\mathcal{L}_1 = \lambda_{\ell_1} \mathcal{L}_{\ell_1} + \lambda_{ssim} \mathcal{L}_{ssim} + \lambda_p \mathcal{L}_p + \lambda_{div} \mathcal{L}_{div} + \lambda_{dc} \mathcal{L}_{dc}$ , where  $\mathcal{L}_{\ell_1}$ ,  $\mathcal{L}_{ssim}$ ,  $\mathcal{L}_p$  are L1, SSIM, and perceptual reconstruction losses,  $\mathcal{L}_{div}$  encourages diverse hypotheses, and  $\mathcal{L}_{dc}$  enforces consistency between predicted and actual degradations. In stage 2, the base model is frozen and the refinement components are trained with a progressive improvement loss:  $\mathcal{L}_2 = \mathcal{L}_{recon} + \lambda_{mag} \|\mathbf{C}\|_1 + \lambda_{imp} \mathcal{L}_{imp}$ , where  $\mathcal{L}_{recon}$  combines L1, SSIM, and perceptual losses,  $\|\mathbf{C}\|_1$  penalizes large corrections, and  $\mathcal{L}_{imp} = \max(0, \|\hat{\mathbf{J}} - \mathbf{J}\|_1 - \|\hat{\mathbf{J}}_1 - \mathbf{J}\|_1 + \epsilon)$  enforces explicit improvement over the base output.

## 4. Experiments

**Experimental Settings.** We evaluate TIDE on three standard underwater image datasets: UIEB [20], EUVP [13], and SUIM-E [33], with all images resized to  $256 \times 256$  for training and testing. We compare against state-of-the-art UIR methods using both full-reference (PSNR, SSIM, LPIPS) and no-reference metrics (UIQM, UISM, BRISQUE), along with UICM and UIConM, which specifically measure color cast correction and local contrast enhancement (detailed experimental settings and metric definitions are provided in the supplementary).

### 4.1. Comparison with State-of-the-Art

Figure 4 and Table 1 show that TIDE achieves consistent improvements across diverse degradations. Existing methods often address specific degradations but fail on others: U-GAN variants restore color but leave haze, FUSION preserves contrast while losing fine details, and DWNet removes haze at the cost of color fidelity, reflecting the challenge of spatially varying, co-occurring degradations in underwater scenes. TIDE mitigates this issue by applying

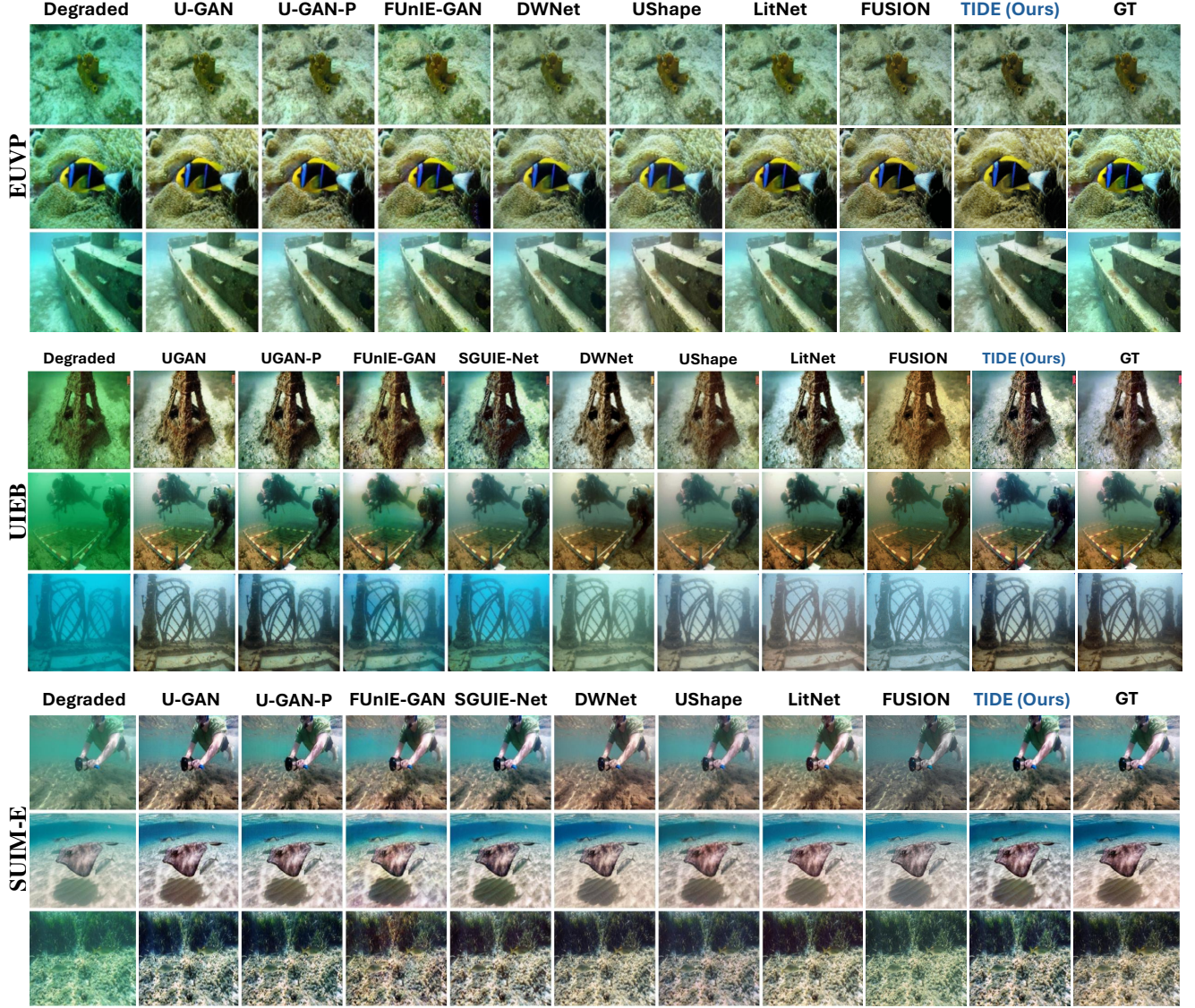


Figure 4. Qualitative restoration results across EUVP, UIEB, and SUIM-E datasets.

degradation-specific processing, yielding balanced restoration in all cases. In the EUVP ship scene (row 3), it recovers low contrast, color distortions, and fine details simultaneously without introducing artifacts. Similarly, in the grass and statue examples from UIEB, TIDE maintains fine textures and structural details while removing color casts, whereas other methods either over-saturate or retain residual haze. Quantitatively, TIDE achieves higher fidelity and perceptual quality, reaching 0.910 SSIM on UIEB (vs. 0.883 for FUSION) and 3.440 UIQM (vs. 3.432 for U-GAN). These results stem from inverse degradation mapping, which disentangles co-occurring distortions, and the refinement stage, which reduces residual artifacts.

To evaluate TIDE under real-world conditions beyond

clear-water datasets, we test it on the RUIE dataset [27] using weights trained on UIEB. We focus on the UIQS and UCCS subsets, which capture naturally turbid scenes with strong color casts. UIEB was chosen for training as it provides sufficient paired data to learn robust enhancement mappings while remaining limited enough to test generalization. For comparison, we include FUSION [45] and LitNet [32], the two strongest baselines from Table 1 to assess both relative performance and generalization. As shown in Fig. 5, TIDE consistently achieves higher UICM (2.13 vs. 0.43 and 0.98) and UIConM (9.28 vs. 5.93 and 7.11) scores. Qualitatively, it better handles heavily distorted regions: in row 1, TIDE restores natural rock textures while correcting the green cast, whereas FUSION introduces yellowish arti-



Table 1. Performance comparison of UIE methods across EUVP, UIEB, and SUIM-E test sets. ↓ indicates lower is better. First, second, and third best performances are represented with red, blue, and green background colors, respectively.

Method	EUVP						UIEB						SUIM-E					
	PSNR	SSIM	UIQM	LPIPS ↓	UISM	BRISQUE ↓	PSNR	SSIM	LPIPS ↓	UIQM	UISM	BRISQUE ↓	PSNR	SSIM	LPIPS ↓	UIQM	UISM	BRISQUE ↓
DWNet [38]	28.654	0.835	3.042	<b>0.173</b>	<b>7.051</b>	<b>30.856</b>	23.165	0.843	0.162	2.897	7.089	24.863	24.850	<b>0.861</b>	<b>0.133</b>	2.707	7.381	20.757
UGAN [8]	26.551	0.807	2.896	0.220	6.833	35.859	23.322	0.815	0.199	<b>3.432</b>	7.241	27.011	24.704	0.826	0.190	2.894	7.175	20.288
UGAN-P [8]	26.549	0.805	2.931	0.223	6.816	35.099	23.550	0.814	0.192	3.396	7.262	25.382	25.050	0.827	0.188	2.901	7.184	<b>18.768</b>
FUSION [45]	<b>28.671</b>	<b>0.862</b>	<b>3.220</b>	0.174	<b>7.048</b>	<b>29.547</b>	<b>23.717</b>	<b>0.883</b>	<b>0.112</b>	<b>3.414</b>	<b>7.429</b>	<b>23.193</b>	<b>25.989</b>	0.850	<b>0.118</b>	<b>3.183</b>	<b>7.679</b>	<b>18.655</b>
Lit-Net [32]	<b>29.477</b>	<b>0.851</b>	3.027	<b>0.169</b>	7.011	32.109	<b>23.603</b>	<b>0.863</b>	<b>0.130</b>	3.145	<b>7.396</b>	<b>23.038</b>	25.117	<b>0.884</b>	<b>0.118</b>	<b>2.918</b>	7.368	19.602
FUnIE-GAN [13]	26.220	0.792	2.971	0.212	6.892	30.912	21.043	0.785	0.173	3.250	7.202	24.522	23.590	0.825	0.189	<b>2.918</b>	7.121	22.560
Ushape [31]	26.822	0.811	<b>3.052</b>	0.187	6.843	35.648	21.084	0.744	0.220	3.161	7.183	24.128	22.647	0.783	0.213	2.873	7.061	22.876
SQUIE-Net [33]	-	-	-	-	-	-	23.496	0.853	0.136	3.004	7.362	24.607	<b>25.987</b>	0.857	0.153	2.637	7.090	25.927
ULAP [39]	-	-	-	-	-	-	19.863	0.724	0.256	2.328	7.362	25.113	19.148	0.744	0.231	2.115	<b>7.475</b>	21.250
TIDE (Ours)	<b>29.469</b>	<b>0.906</b>	<b>3.281</b>	<b>0.159</b>	<b>7.066</b>	<b>29.545</b>	<b>23.753</b>	<b>0.910</b>	<b>0.115</b>	<b>3.440</b>	<b>7.439</b>	<b>22.991</b>	<b>25.987</b>	<b>0.906</b>	<b>0.119</b>	<b>3.195</b>	<b>7.685</b>	<b>18.605</b>

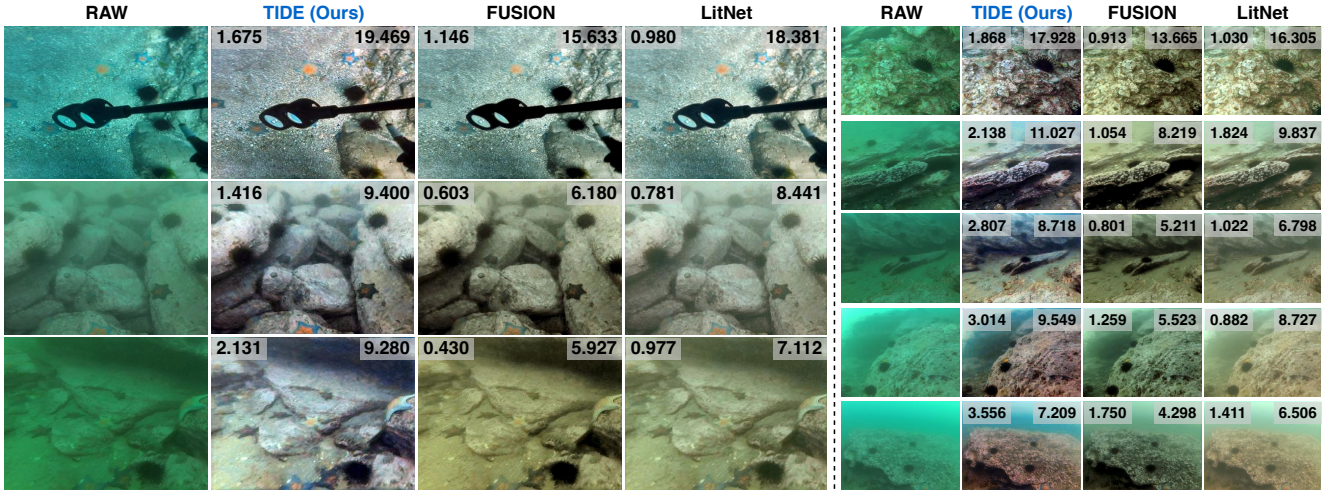


Figure 5. Qualitative comparison on naturally turbid underwater images from the RUIE dataset. The left group corresponds to the UCCS dataset, while the right group corresponds to the UIQS dataset. For each result, the two metrics displayed in the top corners are UICM (left, measuring color correction) and UICoM (right, measuring contrast enhancement). Higher values indicate better performance for both metrics.

facts and LitNet leaves residual haze; in rows 4–5, it yields finer details of marine life with more natural coloration.

## 4.2. Hardware Efficiency Analysis

TIDE achieves remarkable inference efficiency through its architectural design, even with its substantial model size of 115.8M parameters. We evaluate performance on an RTX 4070 Ti SUPER to demonstrate computational efficiency on high-end consumer hardware, representing the upper bound of deployment performance potential. Figure 6 demonstrates that our model achieves real-time performance ( $>30$  FPS) at  $256 \times 256$  resolution with a single batch, and significantly higher throughput (123.4 FPS) at  $128 \times 128$  resolution with batch size 8, while maintaining minimal memory footprint (0.46 GB). This efficiency arises from three design choices: (1) decoupled specialized decoders that process shared features in parallel rather than sequentially; (2) a refinement stage that introduces only 1.1% overhead (1.25M params) by generating sparse corrections instead of full restorations; and (3) degradation-guided fusion that se-

lectively applies computation to degraded regions, avoiding redundant processing in well-preserved areas. This enables TIDE to scale efficiently with batch size: throughput increases from 40.3 FPS to 123.4 FPS when moving from batch size 1 to 8 at  $128 \times 128$  resolution with only a marginal 0.02 GB memory increase, while at  $256 \times 256$  resolution, the model maintains consistent real-time performance ( $\sim 33$  FPS) when scaling from batch size 1 to 4 with minimal memory overhead (0.04 GB  $\uparrow$ ), making it well-suited for both real-time applications and high-throughput batch processing scenarios on modern consumer hardware.

## 4.3. Ablation Study

We conduct a comprehensive ablation study to assess the contribution of each component (Table 2). For the decoders, a color-only variant reaches 22.39 dB PSNR on EUVP but struggles with diverse degradations. Adding additional decoders consistently improves performance, with certain combinations showing clear complementarity: color–detail–denoise achieves 23.33 dB PSNR,



Table 2. Ablation study of TIDE components. Removing specialized decoders, loss terms, or the refinement stage reduces performance across multiple datasets. The metrics displayed are an **average** over all the images in the test set.

Config					EUVP			UIEB			SUIM-E			UIQS		UCCS	
Decoder Types	color	contrast	detail	denoise	LPIPS ↓	PSNR	SSIM	LPIPS ↓	PSNR	SSIM	LPIPS ↓	PSNR	SSIM	UICM	UIConM	UICM	UIConM
	✓	✗	✗	✗	0.216	22.391	0.867	0.158	22.809	0.890	0.158	22.517	0.882	13.451	0.847	13.563	0.862
	✓	✓	✗	✗	0.209	22.623	0.873	0.205	23.333	0.901	0.204	23.216	0.900	13.642	0.894	13.731	0.908
	✓	✗	✓	✗	0.210	22.565	0.872	0.207	23.239	0.899	0.206	23.096	0.898	13.598	0.885	13.694	0.901
	✓	✗	✗	✓	0.207	22.713	0.876	0.203	23.210	0.899	0.207	22.853	0.892	13.683	0.909	13.768	0.923
	✓	✓	✓	✗	0.192	23.252	0.889	0.203	23.494	0.904	0.201	23.365	0.903	14.087	1.012	14.195	1.031
	✓	✓	✓	✓	0.195	23.194	0.888	0.201	23.488	0.902	0.202	23.202	0.900	14.024	0.991	14.138	1.013
	✓	✗	✓	✓	0.190	23.331	0.891	0.200	23.484	0.903	0.205	23.101	0.900	14.145	1.024	14.253	1.045
Loss	No Degradation Consistency				0.354	19.841	0.792	0.228	21.095	0.802	0.252	21.626	0.792	13.205	0.813	13.458	0.826
	No Diversity				0.229	21.231	0.845	0.170	22.701	0.886	0.189	21.853	0.861	13.894	0.962	14.127	0.981
Supervision	Direct Fusion				0.200	22.973	0.882	0.202	23.461	0.903	0.221	23.042	0.897	14.162	1.024	14.297	1.047
	No Degradation Maps				0.223	22.022	0.859	0.295	21.435	0.844	0.255	23.259	0.902	13.733	0.881	13.946	0.902
	Single Hypothesis				0.202	22.868	0.880	0.210	22.740	0.888	0.210	22.494	0.884	13.985	0.953	14.104	0.968
	No Refinement				0.188	23.414	0.892	0.202	23.547	0.904	0.202	23.417	0.905	14.294	1.065	14.385	1.089
Full TIDE					0.159	29.469	0.906	0.115	23.753	0.910	0.119	25.987	0.906	14.647	1.134	14.729	1.107

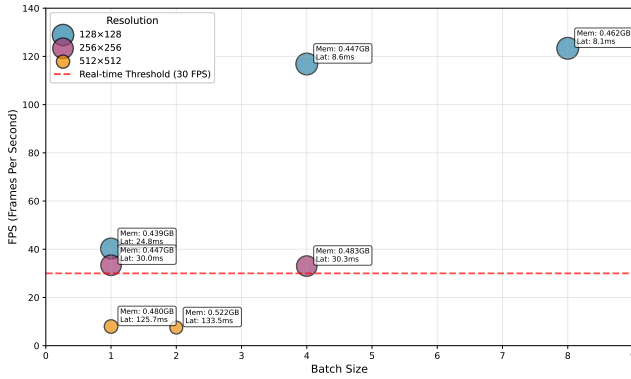


Figure 6. Performance analysis of TIDE across different resolutions and batch sizes on RTX 4070 Ti SUPER. Bubble size indicates processing speed (inverse latency), while position represents the throughput-memory tradeoff. The horizontal red line marks the 30 FPS real-time processing threshold. Even at  $256 \times 256$  resolution, TIDE achieves real-time performance (33.7 FPS) with minimal memory usage (0.44 GB), while smaller resolutions enable substantial throughput improvements with negligible overhead.

slightly higher than color–contrast–detail at 23.25 dB. Similar behavior is observed on turbid datasets, where color–detail–denoise obtains 14.15 and 14.25 UICM on UIQS and UCCS, compared to 13.45 and 13.56 for color-only, indicating that dedicated processing paths are more effective than a single-purpose design. Loss function ablations show that removing degradation consistency or diversity losses substantially reduces performance across all datasets (*e.g.*, LPIPS rises from 0.159 to 0.354 on EUVP without consistency), with particularly large drops on turbid water (UICM decreases from 14.65 to 13.21 on UIQS). Architectural ablations show similar trends: direct fusion in place of adaptive fusion, omitting degradation maps, or using a single hypothesis each reduce performance. Re-

moving the refinement stage results in the most pronounced degradation, with EUVP PSNR dropping by 6.06 dB and UIQS UICM decreasing from 14.65 to 14.29.

**Limitations.** While TIDE demonstrates significant improvements over existing methods, some limitations remain. In scenes with extreme lighting variations (*e.g.*, areas affected simultaneously by direct sunlight and deep shadows), degradation maps may not balance restoration perfectly, potentially causing overprocessing in some regions while leaving subtle degradations in others. This stems from the inherent difficulty of disentangling heavily intertwined degradations rather than our four-category framework. Additionally, TIDE may struggle with uncommon underwater phenomena, such as complex caustics or unusual particulate scattering. Although evaluations on challenging real-world datasets show good generalization, performance could be further enhanced using physics-guided approaches that model these rare optical effects without extensive additional training data.

## 5. Conclusion

We introduced TIDE, a two-stage framework for UIR that addresses spatially varying degradations through inverse degradation mapping with specialized prior decomposition and progressive refinement. By explicitly modeling four fundamental degradation types, TIDE effectively handles the heterogeneous combination of color distortion, contrast reduction, detail loss, and noise in underwater imagery. Experiments across standard benchmarks and challenging turbid water scenarios demonstrate consistent performance improvements in both reference-based metrics and perceptual quality measures. We hope TIDE will inspire future research on more effective underwater image/video processing systems that adapt to diverse degradations, benefiting applications in underwater robotics and archaeological surveys.

## References

- [1] Derya Akkaynak and Tali Treibitz. A revised underwater image formation model. In *2018 IEEE/CVF Conference on Computer Vision and Pattern Recognition*, pages 6723–6732, 2018. 4
- [2] Derya Akkaynak and Tali Treibitz. Sea-thru: A method for removing water from underwater images. In *2019 IEEE/CVF Conference on Computer Vision and Pattern Recognition (CVPR)*, pages 1682–1691, 2019. 4
- [3] Chaofeng Chen, Xiaoming Li, Lingbo Yang, Xianhui Lin, Lei Zhang, and Kwan-Yee K. Wong. Progressive semantic-aware style transformation for blind face restoration. In *2021 IEEE/CVF Conference on Computer Vision and Pattern Recognition (CVPR)*, pages 11891–11900, 2021. 3
- [4] Jie Chen, Zaifeng Yang, Tsz Nam Chan, Hui Li, Junhui Hou, and Lap-Pui Chau. Attention-guided progressive neural texture fusion for high dynamic range image restoration. *IEEE Transactions on Image Processing*, 31:2661–2672, 2022. 3
- [5] Yu-Wei Chen and Soo-Chang Pei. Always clear days: Degradation type and severity aware all-in-one adverse weather removal. *IEEE Access*, 13:7650–7662, 2025. 2
- [6] Xiaofeng Cong, Yu Zhao, Jie Gui, Junming Hou, and Dacheng Tao. A comprehensive survey on underwater image enhancement based on deep learning. *arXiv preprint arXiv:2405.19684*, 2024. 2
- [7] Dazhao Du, Lingyu Si, Fanjiang Xu, Jianwei Niu, and Fuchun Sun. A physical model-guided framework for underwater image enhancement and depth estimation, 2025. 4
- [8] Cameron Fabbri, Md Jahidul Islam, and Junaed Sattar. Enhancing underwater imagery using generative adversarial networks. In *2018 IEEE International Conference on Robotics and Automation (ICRA)*, pages 7159–7165. IEEE, 2018. 1, 7
- [9] Farong Gao, Kai Wang, Zhangyi Yang, Yejian Wang, and Qizhong Zhang. Underwater image enhancement based on local contrast correction and multi-scale fusion. *Journal of Marine Science and Engineering*, 9(2):225, 2021. 2
- [10] Y. R. Gogireddy and J. R. Gogireddy. Advanced underwater image quality enhancement via hybrid super-resolution convolutional neural networks and multi-scale retinex-based defogging techniques. *arXiv preprint arXiv:2410.14285*, 2024. 2
- [11] Ian Goodfellow, Jean Pouget-Abadie, Mehdi Mirza, Bing Xu, David Warde-Farley, Sherjil Ozair, Aaron Courville, and Yoshua Bengio. Generative adversarial nets. *Advances in neural information processing systems*, 27, 2014. 2
- [12] Yecai Guo, Hanyu Li, and Peixian Zhuang. Underwater image enhancement using a multiscale dense generative adversarial network. *IEEE Journal of Oceanic Engineering*, 45(3):862–870, 2019. 2
- [13] Md Jahidul Islam, Youya Xia, and Junaed Sattar. Fast underwater image enhancement for improved visual perception. *IEEE Robotics and Automation Letters*, 5(2):3227–3234, 2020. 2, 5, 7
- [14] J.S. Jaffe. Computer modeling and the design of optimal underwater imaging systems. *IEEE Journal of Oceanic Engineering*, 15(2):101–111, 1990. 4
- [15] P. Jahoda, Y. Yeganeh, E. Adeli, N. Navab, and A. Farshad. PRISM: Progressive Restoration for Scene Graph-Based Image Manipulation. In *Computer Vision – ECCV 2024 Workshops*, pages 137–153. Springer, Cham, 2025. 3
- [16] Aupendu Kar, Sobhan Kanti Dhara, Debashis Sen, and Prabir Kumar Biswas. Zero-shot single image restoration through controlled perturbation of koschmieder’s model. In *Proceedings of the IEEE/CVF Conference on Computer Vision and Pattern Recognition*, pages 16205–16215, 2021. 1
- [17] Naresh Kumar, Juveria Manzar, Shivani, and Shubham Garg. Underwater image enhancement using deep learning. *Multi-media Tools and Applications*, 82:46789–46809, 2023. 2
- [18] Yong Lai, Haiyong Xu, Chi Lin, Ting Luo, and Lihong Wang. A two-stage and two-branch generative adversarial network-based underwater image enhancement. *The Visual Computer*, 39(9):4133–4147, 2023. 2
- [19] Chongyi Li, Jichang Guo, Shanji Chen, Yibin Tang, Yanwei Pang, and Jian Wang. Underwater image restoration based on minimum information loss principle and optical properties of underwater imaging. In *2016 IEEE International Conference on Image Processing (ICIP)*, pages 1993–1997. IEEE, 2016. 2
- [20] Chongyi Li, Chunle Guo, Wenqi Ren, Runmin Cong, Junhui Hou, Sam Kwong, and Dacheng Tao. An underwater image enhancement benchmark dataset and beyond. *IEEE Transactions on Image Processing*, 29:4376–4389, 2019. 2, 5
- [21] Chongyi Li, Saeed Anwar, Junhui Hou, Runmin Cong, Chunle Guo, and Wenqi Ren. Underwater image enhancement via medium transmission-guided multi-color space embedding. *IEEE Transactions on Image Processing*, 30:4985–5000, 2021. 1, 2
- [22] Jie Li, Katherine A. Skinner, Ryan M. Eustice, and Matthew Johnson-Roberson. Watergan: Unsupervised generative network to enable real-time color correction of monocular underwater images. *IEEE Robotics and Automation Letters*, page 1–1, 2017. 1
- [23] Jie Li, Lei Zhao, Heng Li, Xiaojun Xue, and Hui Liu. Mixrformer: Dual-branch network for underwater image enhancement in wavelet domain. *Sensors*, 25(11):3302, 2025. 2
- [24] B. Liu, X. Ning, S. Ma, and Y. Yang. Multi-scale dense spatially-adaptive residual distillation network for lightweight underwater image super-resolution. *Frontiers in Marine Science*, 10:1328436, 2023. 2
- [25] M. Liu, X. Su, X. Yao, W. Hao, and W. Zhu. Lensless image restoration based on multi-stage deep neural networks and pix2pix architecture. *Photonics*, 10(11):1274, 2023. 3
- [26] Peng Liu, Guoyu Wang, Hao Qi, Chufeng Zhang, Haiyong Zheng, and Zhibin Yu. Underwater image enhancement with a deep residual framework. *IEEE Access*, 7:94614–94629, 2019. 2
- [27] Risheng Liu, Xin Fan, Ming Zhu, Minjun Hou, and Zhongxuan Luo. Real-world underwater enhancement: Challenges, benchmarks, and solutions, 2019. 6, 5

- [28] Shuai Liu, Peng Chen, Jianyu Lan, Jianru Li, Zhengxiang Shen, and Zhanshan Wang. Underwater image restoration via multiscale optical attenuation compensation and adaptive dark channel dehazing. *Computers and Electrical Engineering*, 123:110228, 2025. 2
- [29] Tong Liu, Kaiyan Zhu, Weiye Cao, Bolin Shan, and Fangyi Guo. Zero-umsie: a zero-shot underwater multi-scale image enhancement method based on isomorphic features. *Optics Express*, 32(23):40398–40415, 2024. 1
- [30] Prashant W. Patil, Sunil Gupta, Santu Rana, Svetha Venkatesh, and Subrahmanyam Murala. Multi-weather image restoration via domain translation. In *2023 IEEE/CVF International Conference on Computer Vision (ICCV)*, pages 21639–21648, 2023. 2
- [31] Lintao Peng, Chunli Zhu, and Liheng Bian. U-shape transformer for underwater image enhancement. *IEEE Transactions on Image Processing*, 2023. 7
- [32] Alik Pramanick, Arijit Sur, and V Vijaya Saradhi. Harnessing multi-resolution and multi-scale attention for underwater image restoration. *The Visual Computer*, pages 1–20, 2025. 2, 6, 7
- [33] Qi Qi, Kunqian Li, Haiyong Zheng, Xiang Gao, Guojia Hou, and Kun Sun. Sguie-net: Semantic attention guided underwater image enhancement with multi-scale perception. *IEEE Transactions on Image Processing*, 31:6816–6830, 2022. 5, 7
- [34] Cheng Qian, Wang Yinmin, and Liu Yao. Image restoration of highly reflective polarization targets in turbid media based on circularly polarized light. *IEEE Access*, 12: 184657–184666, 2024. 4
- [35] Nianzu Qiao and Lamei Di. Underwater image enhancement combining low-dimensional and global features. *The Visual Computer*, 39(7):3029–3039, 2023. 2
- [36] Dongwei Ren, Wangmeng Zuo, Qinghua Hu, Pengfei Zhu, and Deyu Meng. Progressive image deraining networks: A better and simpler baseline. In *2019 IEEE/CVF Conference on Computer Vision and Pattern Recognition (CVPR)*, pages 3932–3941, 2019. 2
- [37] Y.Y. Schechner and N. Karpel. Clear underwater vision. In *Proceedings of the 2004 IEEE Computer Society Conference on Computer Vision and Pattern Recognition, 2004. CVPR 2004.*, pages I–I, 2004. 4
- [38] Prasen Sharma, Ira Bisht, and Arijit Sur. Wavelength-based attributed deep neural network for underwater image restoration. *ACM Transactions on Multimedia Computing, Communications and Applications*, 19(1):1–23, 2023. 7
- [39] Wei Song, Yan Wang, Dongmei Huang, and Dian Tjondronegoro. A rapid scene depth estimation model based on underwater light attenuation prior for underwater image restoration. In *Advances in Multimedia Information Processing—PCM 2018: 19th Pacific-Rim Conference on Multimedia, Hefei, China, September 21–22, 2018, Proceedings, Part I 19*, pages 678–688. Springer, 2018. 7
- [40] Jan Sticklus, Martin Hieronymi, and Peter Adam Hoehner. Effects and constraints of optical filtering on ambient light suppression in led-based underwater communications. *Sensors*, 18(11):3710, 2018. 4
- [41] Kaichuan Sun and Yubo Tian. Dbfnnet: A dual-branch fusion network for underwater image enhancement. *Remote Sensing*, 15(5):1195, 2023. 2
- [42] Zhijie Tang, Jianda Li, Jingke Huang, Zhanhua Wang, and Zhihang Luo. Multi-scale convolution underwater image restoration network. *Machine Vision and Applications*, 33(6):85, 2022. 2
- [43] Ye Tao, Jinhui Tang, Xinwei Zhao, Chen Zhou, Chong Wang, and Zhonglei Zhao. Multi-scale network with attention mechanism for underwater image enhancement. *Neurocomputing*, page 127926, 2024. 2
- [44] Hamidreza Farhadi Tolia, Jinchang Ren, and Eyad Elyan. Dicam: Deep inception and channel-wise attention modules for underwater image enhancement. *Neurocomputing*, 584: 127585, 2024. 2
- [45] Jaskaran Singh Walia, Shravan Venkatraman, and Pavithra LK. Fusion: Frequency-guided underwater spatial image reconstruction, 2025. 2, 6, 7
- [46] Bowen Wang, Zhi Wang, Wenhui Guo, and Yanjiang Wang. A dual-branch joint learning network for underwater object detection. *Knowledge-Based Systems*, 293:111672, 2024. 2
- [47] Meng Wang, Jizheng Xu, Li Zhang, Junru Li, and Shiqi Wang. Multi-hypothesis inspired super-resolution for compression distorted screen content image. In *Applications of Digital Image Processing XLIV (Proc. SPIE)*, page 1184206. SPIE, 2021. 3
- [48] Shengcong Wu, Ting Luo, Gangyi Jiang, Mei Yu, Haiyong Xu, Zhongjie Zhu, and Yang Song. A two-stage underwater enhancement network based on structure decomposition and characteristics of underwater imaging. *IEEE Journal of Oceanic Engineering*, 46(4):1213–1227, 2021. 2
- [49] Qiang Xie, Xiujing Gao, Zhen Liu, and Hongwu Huang. Underwater image enhancement based on zero-shot learning and level adjustment. *Heliyon*, 9(4), 2023. 1
- [50] Zexuan Xing, Haiyong Xu, Gangyi Jiang, Mei Yu, Ting Luo, and Yeyao Chen. Vision graph convolutional network for underwater image enhancement. *Knowledge-Based Systems*, 299:112048, 2024. 2
- [51] Peng Yang, Heng Wu, Chunhua He, and Shaojuan Luo. Underwater image restoration for seafloor targets with hybrid attention mechanisms and conditional generative adversarial network. *Digital Signal Processing*, 134:103900, 2023. 2
- [52] Syed Waqas Zamir, Aditya Arora, Salman Khan, Munawar Hayat, Fahad Shahbaz Khan, Ming-Hsuan Yang, and Ling Shao. Multi-stage progressive image restoration. In *2021 IEEE/CVF Conference on Computer Vision and Pattern Recognition (CVPR)*, pages 14816–14826, 2021. 2
- [53] Jinghao Zhang, Jie Huang, Mingde Yao, Zizheng Yang, Hu Yu, Man Zhou, and Feng Zhao. Ingredient-oriented multi-degradation learning for image restoration. In *2023 IEEE/CVF Conference on Computer Vision and Pattern Recognition (CVPR)*, pages 5825–5835, 2023. 2
- [54] Y. Zhang, J. Li, H. Wang, Y. Zhang, and Y. Wang. Dae-gan: Underwater image super-resolution based on symmetric dual attention and edge enhancement. *Symmetry*, 16(5):588, 2024. 2



- [55] Yanwen Zhang, Ziran Li, and Akio Namiki. Redundant feature-processing module based on dual-branch for underwater image enhancement. *IEEE Transactions on Instrumentation and Measurement*, 2024. 2
- [56] Yi Zhang, Qixue Yang, Damon M. Chandler, and Xuanqin Mou. Reference-based multi-stage progressive restoration for multi-degraded images. *IEEE Transactions on Image Processing*, 33:4982–4997, 2024. 3
- [57] Jianhua Zheng, Ruolin Zhao, Gaolin Yang, Shuangyin Liu, Zihao Zhang, Yusha Fu, and Junde Lu. An underwater image restoration deep learning network combining attention mechanism and brightness adjustment. *Journal of Marine Science and Engineering*, 12(1):7, 2023. 2

# TIDE: Two-Stage Inverse Degradation Estimation with Guided Prior Disentanglement for Underwater Image Restoration

## Supplementary Material

### A1. Extended Methodology

In this section, we provide detailed elaboration of our Two-stage Inverse Degradation Estimation (TIDE) framework. We describe the architectural components, fusion mechanisms, and optimization strategies that enable effective underwater image restoration through degradation-aware processing.

#### A1.1. Network Architecture and Component Details

Our framework builds upon a multi-scale feature extraction backbone coupled with specialized processing modules. Here we provide a detailed examination of each component’s internal structure and mathematical formulation.

The feature extraction module  $\mathcal{E}$  employs a hierarchical encoder structure with  $N$  downsampling operations, generating feature maps at progressively lower resolutions. For an input image  $\mathbf{I} \in \mathbb{R}^{3 \times H \times W}$ , the initial features are extracted via:

$$\mathbf{f}_0 = \phi(\mathbf{I}, \mathbf{W}_0, \mathbf{b}_0) \quad (4)$$

where  $\phi$  represents a convolution operation with normalization and non-linear activation, parameterized by weights  $\mathbf{W}_0$  and bias  $\mathbf{b}_0$ . Subsequent feature maps are computed recursively as  $\mathbf{f}_i = \psi(\mathbf{f}_{i-1}, \mathbf{W}_i, \mathbf{b}_i)$  for  $i \in \{1, 2, \dots, N\}$ , where  $\psi$  incorporates strided convolution for downsampling. At the bottleneck, we apply multiple residual blocks to enhance feature representation without altering spatial dimensions:

$$\mathbf{f}_N = \mathbf{f}_N + \sum_{j=1}^R \rho_j(\mathbf{f}_N) \quad (5)$$

where  $\rho_j$  represents the  $j$ -th residual block with  $R = 2$  in our implementation. The complete feature hierarchy  $\mathbf{F} = \{\mathbf{f}_0, \mathbf{f}_1, \dots, \mathbf{f}_N\}$  captures multi-scale information critical for addressing different degradation types.

The degradation estimation module  $\mathcal{D}$  implements a lightweight encoder-decoder structure augmented with a global context module. The encoder follows a similar hierarchical design as  $\mathcal{E}$  but with fewer channels, generating a compact feature representation  $\mathbf{z}_N$ . The global context module enhances this representation by modeling long-range dependencies:

$$\mathbf{g} = \mathbf{z}_N \odot \sigma(W_2(\delta(W_1(\text{GAP}(\mathbf{z}_N)))))) \quad (6)$$

where GAP denotes global average pooling,  $W_1$  and  $W_2$  are linear transformations,  $\delta$  is ReLU activation, and  $\sigma$  is sigmoid activation. This global context  $\mathbf{g}$  is concatenated with  $\mathbf{z}_N$  before progressive upsampling with skip connections from the encoder. The final degradation maps  $\mathbf{M} \in \mathbb{R}^{K \times H \times W}$  are computed as:

$$\mathbf{M} = \sigma(W_o(\mathbf{u}_0)) \quad (7)$$

where  $\mathbf{u}_0$  is the final upsampled feature map and  $W_o$  is a  $1 \times 1$  convolution projecting to  $K$  channels, followed by sigmoid activation to ensure  $M_k(x, y) \in [0, 1]$ .

#### A1.2. Degradation Types and Specialized Decoders

We decompose underwater image degradation into four fundamental types based on the physical processes affecting underwater light propagation:

1. **Color distortion:** Caused by wavelength-dependent attenuation where red light (longer wavelengths) is absorbed more rapidly than green and blue light (shorter wavelengths), resulting in the characteristic blue-green color cast of underwater images.
2. **Contrast reduction:** Results from light scattering by suspended particles, creating haze and reducing the dynamic range of the image, particularly at greater depths or in turbid waters.
3. **Detail loss:** Occurs due to medium absorption and forward scattering effects that blur fine structures and high-frequency details, especially at increasing distances from the camera.
4. **Noise:** Originates from sensor limitations in low-light underwater conditions and from optical effects of suspended particles such as marine snow.

For each degradation type, we design a specialized decoder with architectural inductive biases that naturally guide it toward addressing its target degradation without requiring explicit degradation-specific supervision. Algorithm 1 outlines the general structure of our specialized decoders.

The specialized processing functions for each decoder are designed with inductive biases tailored to their target degradation types:

**Color Restoration Decoder.** The color decoder implements channel-wise attention mechanisms at multiple scales to recalibrate color-specific features. For feature map  $\mathbf{x} \in \mathbb{R}^{C \times h \times w}$  at scale  $i$ , the specialized processing computes:

---

**Algorithm 1** Specialized Restoration Decoder

---

**Require:** Hierarchical features  $\mathbf{F} = \{\mathbf{f}_0, \mathbf{f}_1, \dots, \mathbf{f}_N\}$

**Ensure:** Restoration hypothesis  $\mathbf{H} \in \mathbb{R}^{3 \times H \times W}$

```
 $\mathbf{x} \leftarrow \mathbf{f}_N$  {Start with bottleneck features}  
for  $i = N - 1$  down to 0 do  
   $\mathbf{x} \leftarrow \text{Upsample}(\mathbf{x})$  {2× bilinear upsampling}  
   $\mathbf{x} \leftarrow \text{Concatenate}(\mathbf{x}, \mathbf{f}_i)$  {Skip connection}  
   $\mathbf{x} \leftarrow \phi_i(\mathbf{x})$  {Channel calibration convolution}  
   $\mathbf{x} \leftarrow \text{SpecializedProcessing}_i(\mathbf{x})$  {Decoder-specific processing}  
end for  
 $\mathbf{x} \leftarrow \phi_{\text{out}}(\mathbf{x})$  {Output convolution}  
 $\mathbf{H} \leftarrow (\tanh(\mathbf{x}) + 1)/2$  {Range normalization to [0,1]}  
return  $\mathbf{H}$ 
```

---

$$\text{SpecializedProcessing}_i(\mathbf{x}) = \mathbf{x} \odot \sigma(W_{2,i}(\delta(W_{1,i}(\mathbf{x})))) \quad (8)$$

where  $W_{1,i} : \mathbb{R}^C \rightarrow \mathbb{R}^{C/r}$  and  $W_{2,i} : \mathbb{R}^{C/r} \rightarrow \mathbb{R}^C$  are learned projections with reduction ratio  $r = \max(4, C/16)$ . This squeeze-and-excitation attention structure excels at addressing wavelength-dependent color distortions that affect different color channels non-uniformly.

**Contrast Enhancement Decoder.** The contrast decoder uses residual blocks designed to enhance local contrast while preserving structural information:

$$\text{SpecializedProcessing}_i(\mathbf{x}) = \mathbf{x} + \phi_{c,i}(\mathbf{x}) \quad (9)$$

where  $\phi_{c,i}$  consists of convolutional layers with normalization and non-linear activation. This architecture is particularly effective at countering the haze and contrast reduction caused by light scattering, as it can amplify local contrast variations without introducing artifacts.

**Detail Recovery Decoder.** The detail decoder employs cascaded residual blocks specifically designed for high-frequency information recovery:

$$\text{SpecializedProcessing}_i(\mathbf{x}) = \mathbf{x} + \sum_{j=1}^L \phi_{d,i,j}(\mathbf{x}) \quad (10)$$

where  $L = 2$  and each  $\phi_{d,i,j}$  represents a residual block with edge-preserving operations. This cumulative enhancement approach is particularly suited for recovering fine details lost through medium absorption, as it progressively refines high-frequency components while maintaining structural coherence.

**Denoising Decoder.** The noise decoder utilizes group convolutions to exploit local correlations while preserving structural information:

$$\text{SpecializedProcessing}_i(\mathbf{x}) = \text{Conv}_{1 \times 1}(\text{GConv}_{3 \times 3}(\phi_{n,i}(\mathbf{x}))) \quad (11)$$

where  $\text{GConv}_{3 \times 3}$  denotes group convolution with  $g = \min(\lfloor C/8 \rfloor, C)$  groups, allowing specialized filtering within channel subgroups, followed by a  $1 \times 1$  convolution for cross-group information exchange. This architecture is particularly effective for handling the noise from suspended particles while preserving important image structures.

### A1.3. Fusion and Progressive Refinement Mechanisms

Our framework incorporates two fusion mechanisms: adaptive hypothesis fusion in the first stage and safety-gated refinement fusion in the second stage. Additionally, we implement a differential degradation analysis for targeted refinement.

**Adaptive Hypothesis Fusion.** The base model combines multiple restoration hypotheses  $\{H_1, H_2, \dots, H_K\}$  using degradation-guided weights. We implement three fusion variants, with learned fusion being our primary approach. The direct fusion establishes a one-to-one mapping between degradation maps and hypotheses:

$$\hat{\mathbf{J}}_1 = \sum_{k=1}^K M_k \odot H_k \quad (12)$$

assuming  $K$  degradation types correspond directly to  $K$  hypotheses. In contrast, our learned fusion approach implements a non-linear mapping from degradation maps to fusion weights:

$$\mathbf{W} = \text{softmax}(f_W(\mathbf{M})) \quad (13)$$

where  $f_W$  consists of convolutional layers with residual connections, and the softmax ensures that weights sum to 1 at each spatial location. The fused output is then:

$$\hat{\mathbf{J}}_1 = \sum_{k=1}^K W_k \odot H_k \quad (14)$$

This learned mapping enables more complex relationships between degradation characteristics and restoration strategies, adapting to various underwater scenes.

**Residual Degradation Analysis.** The second stage begins with analyzing residual degradations after initial



---

**Algorithm 2** Expert-guided Refinement Generation

---

**Require:** Original image  $\mathbf{I}$ , initial restoration  $\hat{\mathbf{J}}_1$ , expert type  $k$

**Ensure:** Correction term  $\mathbf{C}_k$

```

 $\mathbf{x} \leftarrow \text{Concatenate}(\mathbf{I}, \hat{\mathbf{J}}_1)$  {6-channel input}
 $\mathbf{x} \leftarrow \phi_{\text{init},k}(\mathbf{x})$  {Initial feature extraction}
 $\mathbf{x} \leftarrow \phi_{\text{res1},k}(\mathbf{x}) + \mathbf{x}$  {First residual block}
 $\mathbf{x} \leftarrow \phi_{\text{res2},k}(\mathbf{x}) + \mathbf{x}$  {Second residual block}
if  $k = \text{color}$  then
     $\mathbf{x} \leftarrow \phi_{\text{color}}(\mathbf{x})$  {Color-specific processing}
else if  $k = \text{contrast}$  then
     $\mathbf{x} \leftarrow \phi_{\text{contrast}}(\mathbf{x})$  {Contrast-specific processing}
else if  $k = \text{detail}$  then
     $\mathbf{x} \leftarrow \phi_{\text{detail}}(\mathbf{x})$  {Detail-specific processing}
else if  $k = \text{noise}$  then
     $\mathbf{x} \leftarrow \phi_{\text{noise}}(\mathbf{x})$  {Noise-specific processing}
end if
 $\mathbf{C}_k \leftarrow \tanh(\mathbf{x}) \cdot \sigma(s_k)$  {Apply adaptive scaling}
return  $\mathbf{C}_k$ 

```

---

restoration. We formulate this as a difference-guided estimation process that takes both the original degraded image  $\mathbf{I}$  and initial restoration  $\hat{\mathbf{J}}_1$  as inputs:

$$\mathbf{M}_r = \mathcal{D}_2(\mathbf{I}, \hat{\mathbf{J}}_1) \quad (15)$$

The residual estimator  $\mathcal{D}_2$  first computes an absolute difference map  $\mathbf{D} = |\mathbf{I} - \hat{\mathbf{J}}_1|$  that highlights regions with significant changes. A difference enhancement module processes this map to create an attention signal:

$$\mathbf{A} = \sigma(f_d(\mathbf{D})) \quad (16)$$

where  $f_d$  consists of convolutional layers that extract meaningful patterns from the difference map. The concatenated input  $[\mathbf{I}, \hat{\mathbf{J}}_1]$  is processed through an encoder-decoder network whose features are modulated by the attention signal:

$$\mathbf{z} = f_r([\mathbf{I}, \hat{\mathbf{J}}_1]) \odot (1 + \alpha \cdot \mathbf{A}) \quad (17)$$

where  $f_r$  is the residual estimation network and  $\alpha$  is a learnable parameter that controls the influence of the difference enhancement. The final residual degradation maps are obtained by applying a  $1 \times 1$  convolution followed by sigmoid activation:

$$\mathbf{M}_r = \sigma(W_r(\mathbf{z})) \quad (18)$$

**Expert-guided Refinement.** For each residual degradation type, we design a specialized refinement expert that generates targeted corrections. Algorithm 2 outlines the refinement process for each expert.

Each expert implements specialized processing tailored to its degradation type:

- **Color refinement expert** focuses on correcting residual color distortions through sequential convolutions that maintain spatial dimensions while refining color relationships.
- **Contrast refinement expert** enhances local contrast through a combination of standard convolutions and a residual block that preserves structural integrity.
- **Detail refinement expert** employs a more complex pathway with channel expansion and multiple residual connections:

$$\phi_{\text{detail}}(\mathbf{x}) = \text{Conv}_{1 \times 1}(\phi_3(\phi_2(\phi_1(\mathbf{x}) + \mathbf{x}) + \phi_1(\mathbf{x})) + \phi_2(\phi_1(\mathbf{x}))) \quad (19)$$

where  $\phi_1$ ,  $\phi_2$ , and  $\phi_3$  are convolutional layers with normalization and activation.

- **Noise refinement expert** utilizes group convolutions with multiple paths:

$$\phi_{\text{noise}}(\mathbf{x}) = \text{Conv}_{1 \times 1}(\text{GConv}_{3 \times 3}(\phi_n(\mathbf{x}))) \quad (20)$$

with groups  $g = \min(C/4, C)$  to process channel subsets independently.

Each expert produces a correction term  $\mathbf{C}_k$  with adaptive scaling controlled by a learnable parameter  $s_k$ . The scaling ensures that corrections remain moderate and prevents over-correction.

**Safety-gated Fusion.** The individual correction terms are combined through a residual degradation-guided fusion with an additional safety mechanism:

$$\mathbf{W}_r = \text{softmax}(f_r(\mathbf{M}_r)) \quad (21)$$

where  $f_r$  is a mapping function consisting of convolutional layers that transform residual degradation maps into fusion weights. The fused correction is computed as:

$$\mathbf{C}' = \sum_{k=1}^K (W_r)_k \odot \mathbf{C}_k \quad (22)$$

To prevent unnecessary corrections in well-restored regions, we implement a safety gate that examines the initial restoration:

$$G(\hat{\mathbf{J}}_1) = \sigma(f_g(\hat{\mathbf{J}}_1)) \quad (23)$$

where  $f_g$  consists of convolutional layers that identify regions requiring minimal correction. The safety gate produces a spatial mask  $G \in \mathbb{R}^{1 \times H \times W}$  with values in  $[0, 1]$ , where lower values indicate well-restored regions. The final correction is modulated by this gate and a global scaling factor:

$$\mathbf{C} = \mathbf{C}' \odot G(\hat{\mathbf{J}}_1) \cdot \sigma(s_g) \quad (24)$$

where  $s_g$  is a learnable parameter controlling the overall refinement intensity. The final restoration is obtained by:

$$\hat{\mathbf{J}} = \text{clamp}(\hat{\mathbf{J}}_1 + \mathbf{C}, 0, 1) \quad (25)$$

ensuring that the pixel values remain within the valid range.

#### A1.4. Specialization Through Architecture and Loss Functions

A key aspect of our approach is how specialization emerges without explicit supervision for each degradation type. This is achieved through a combination of architectural inductive biases and specialized loss functions.

**Architectural Inductive Biases.** Each decoder and refinement expert incorporates architectural elements specifically designed for its target degradation type:

- The color restoration decoder’s channel attention mechanism is particularly effective for addressing wavelength-dependent color distortions because it can selectively recalibrate different color channels with varying intensities.
- The contrast enhancement decoder’s residual blocks are designed to amplify local contrast variations while preserving structural integrity, making them well-suited for addressing the haze and low contrast caused by light scattering.
- The detail recovery decoder’s cascaded residual structure with multiple pathways excels at recovering high-frequency information lost through medium absorption and forward scattering.
- The denoising decoder’s group convolutions enable specialized filtering within channel subgroups followed by cross-group information exchange, which is particularly effective for removing noise while preserving important image structures.

These architectural choices provide implicit guidance for each decoder to specialize in its target degradation type, even without explicit supervision signals.

**Specialized Loss Functions.** We reinforce this specialization through carefully designed loss functions during training:

- **Diversity Loss:** By explicitly penalizing similarity between different hypotheses, this loss encourages each decoder to develop unique restoration capabilities:

$$\mathcal{L}_{div} = \frac{1}{K(K-1)/2} \sum_{i=1}^K \sum_{j=i+1}^K \text{cos\_sim}(H_i, H_j) \quad (26)$$

where  $\text{cos\_sim}(H_i, H_j)$  computes the cosine similarity between flattened hypothesis tensors. This loss is minimized when hypotheses are orthogonal, encouraging specialization.

- **Degradation Consistency Loss:** This loss ensures that the estimated degradation maps correlate with actual degradations:

$$\mathcal{L}_{dc} = \|\text{norm}(\mathbf{M}_{sum}) - \text{norm}(\|\mathbf{I} - \mathbf{J}\|_1)\|_2^2 \quad (27)$$

where  $\mathbf{M}_{sum} = \sum_{k=1}^K M_k$  is the summed degradation map, and  $\text{norm}(\cdot)$  normalizes the values to  $[0, 1]$  range. This guides the degradation estimator to produce meaningful maps that reflect the spatial distribution and severity of degradations.

Through the combination of these architectural inductive biases and specialized loss functions, each decoder naturally develops specialization in addressing its target degradation type without requiring explicit degradation-specific supervision.

#### A1.5. Loss Functions and Training Strategy

We employ a multi-stage training strategy with carefully designed loss functions to ensure effective learning at each stage.

**Base Model Training.** The first stage trains only the base model with a combination of five loss components:

$$\mathcal{L}_1 = \lambda_{\ell_1} \mathcal{L}_{\ell_1} + \lambda_{ssim} \mathcal{L}_{ssim} + \lambda_p \mathcal{L}_p + \lambda_{div} \mathcal{L}_{div} + \lambda_{dc} \mathcal{L}_{dc} \quad (28)$$

The reconstruction losses include L1 loss, SSIM loss, and perceptual loss:

$$\mathcal{L}_{\ell_1} = \|\hat{\mathbf{J}}_1 - \mathbf{J}\|_1 \quad (29)$$

$$\mathcal{L}_{ssim} = 1 - \text{SSIM}(\hat{\mathbf{J}}_1, \mathbf{J}) \quad (30)$$

$$\mathcal{L}_p = \sum_l \lambda_l \|\Phi_l(\hat{\mathbf{J}}_1) - \Phi_l(\mathbf{J})\|_1 \quad (31)$$

where  $\mathbf{J}$  is the ground truth reference image, SSIM is the structural similarity index, and  $\Phi_l$  represents the  $l$ -th layer features of a pre-trained VGG-19 network.

We also apply auxiliary losses to individual hypotheses:

$$\mathcal{L}_{aux} = \frac{1}{K} \sum_{k=1}^K \|\mathbf{H}_k - \mathbf{J}\|_1 \quad (32)$$

encouraging each hypothesis to approximate the reference image, though with less weight than the primary losses.

**Refinement Stage Training.** In the second stage, we freeze the base model parameters and train only the refinement components using:

$$\mathcal{L}_2 = \mathcal{L}_{recon} + \lambda_{mag}\mathcal{L}_{mag} + \lambda_{imp}\mathcal{L}_{imp} \quad (33)$$

The reconstruction loss  $\mathcal{L}_{recon}$  combines L1, SSIM, and perceptual losses for the final output  $\hat{\mathbf{J}}$ , similar to the first stage. The magnitude loss penalizes excessive correction:

$$\mathcal{L}_{mag} = \|\mathbf{C}\|_1 \quad (34)$$

encouraging minimal refinement where possible. The progressive improvement loss explicitly requires the final output to be better than the initial restoration:

$$\mathcal{L}_{imp} = \max(0, \|\hat{\mathbf{J}} - \mathbf{J}\|_1 - \|\hat{\mathbf{J}}_1 - \mathbf{J}\|_1 + \epsilon) \quad (35)$$

where  $\epsilon = 0.01$  is a small constant that encourages a minimum level of improvement. This loss is activated only when the final restoration has higher error than the initial restoration, penalizing cases where refinement degrades quality.

**Training Strategy.** We implement a two-phase training strategy:

1. **Base Model Training:** We train the degradation estimation, hypothesis generation, and fusion components for 300 epochs using the Adam optimizer with an initial learning rate of  $10^{-4}$  and cosine annealing schedule.

2. **Refinement Training:** With the base model frozen, we train the residual estimation and refinement components for 100 epochs with a reduced learning rate of  $5 \times 10^{-5}$ .

This staged approach ensures stable learning, with each component trained to fulfill its specific role in the restoration pipeline. During inference, the model processes images in a single forward pass through both stages, with negligible additional computational cost for the refinement stage compared to single-stage approaches.

## A2. Experimental Setup and Implementation Details

### A2.1. Training Configuration

We implement our TIDE framework in PyTorch and conduct all experiments on a single NVIDIA RTX 4070 Ti SUPER GPU. For network optimization, we employ a multi-stage training strategy with carefully tuned hyperparameters. In the base model training phase, we use the Adam optimizer with an initial learning rate of  $1 \times 10^{-4}$ , weight decay of  $1 \times 10^{-4}$ , and train for 300 epochs with a batch size of 16. We apply cosine annealing with warm restarts for the learning rate schedule, with cycle length of 50 epochs. During the refinement stage training, we freeze the base

model parameters and train the refinement components for 100 epochs using a reduced learning rate of  $5 \times 10^{-5}$  while maintaining the same optimizer configuration.

We determine the optimal loss function weights through a grid search for hyperparameter tuning. During base model training, we use  $\lambda_{\ell_1} = 1.0$ ,  $\lambda_{ssim} = 0.1$ ,  $\lambda_{perceptual} = 0.1$ ,  $\lambda_{diversity} = 0.05$ , and  $\lambda_{degradation} = 0.1$ . In the refinement stage, we set  $\lambda_{recon} = 1.0$ ,  $\lambda_{magnitude} = 0.1$ , and  $\lambda_{improve} = 0.5$ . For the progressive combined loss during fine-tuning, we balance the base and refinement objectives with  $\lambda_{base} = 0.7$  and  $\lambda_{refinement} = 1.0$ . We apply gradient clipping with a threshold of 1.0 during all training phases to ensure stable convergence. Mixed precision training is employed to improve computational efficiency while maintaining numerical stability.

### A2.2. Network Architecture

The feature extraction backbone consists of 5 downsampling layers starting with 64 base channels and doubling the channel count at each downsampling step up to a maximum of 512 channels. The degradation estimation module employs a lightweight structure with 32 base channels and 4 degradation types corresponding to color distortion, contrast reduction, detail loss, and noise. For normalization, we use instance normalization throughout the network, and LeakyReLU with slope 0.2 as the activation function. The specialized decoders share the same general architecture but incorporate domain-specific processing blocks as detailed in Section A1.

The fusion mechanism implements our learned mapping approach by default, though we also explore a direct fusion alternative in our ablation studies. The residual degradation estimator uses a condensed encoder-decoder structure with 2 downsampling layers, while each refinement expert employs adaptive scaling parameters initialized to 0.1 to ensure gradual refinement during early training. The safety gate in the refinement fusion module uses 16 intermediate channels to generate the spatial modulation mask.

### A2.3. Dataset Details

We conduct experiments on three widely-used underwater image datasets for training and standard evaluation: UIEB [20], EUVP [13], and SUIM-E [33]. Additionally, we include the RUIE dataset [27] specifically to evaluate performance on turbid water conditions.

**Standard Benchmark Datasets.** The EUVP dataset provides 11,435 paired images for training and 515 pairs for testing, all at the same resolution. From the UIEB dataset, which contains 890 paired images, we follow the protocol in [20] by selecting 800 images for training and using the remaining 90 for testing. The SUIM-E dataset consists of 1,635 images, where 1,525 images are used for training and



110 are reserved for evaluation, following the procedure in [32].

**Turbid Water Evaluation.** To evaluate TIDE under challenging real-world conditions beyond clear-water scenarios, we utilize the RUIE dataset [27], focusing on its UIQS (Underwater Image Quality Set) and UCCS (Underwater Color Cast Set) subsets. The UIQS subset comprises 3,630 images of real-world underwater scenes systematically grouped into five quality levels (A–E) based on the UCIQE metric, which quantifies image quality using chromaticity, saturation, and contrast measurements. This graded organization enables comprehensive assessment across varying degrees of turbidity and visual degradation. The UCCS subset contains 300 images selected from UIQS, specifically targeting color restoration capabilities. These images are equally divided into three groups - bluish, greenish/yellowish, and blue-green - each corresponding to common underwater color cast conditions encountered in practice.

For turbid water evaluation, we use the model trained on UIEB without any fine-tuning or domain adaptation, allowing us to assess both relative performance and generalization capabilities. This approach tests whether the model can generalize to significantly more challenging underwater environments with optical properties different from those represented in the training data. We compare TIDE against FUSION [45] and LitNet [32], the two strongest baselines from our main experiments, using both quantitative metrics (UICM and UIConM) and qualitative visual assessments focused on color correction, contrast enhancement, and detail preservation in turbid conditions.

#### A2.4. Turbid Water Evaluation Metrics

For turbid water evaluation, we utilize metrics specifically designed to assess underwater image quality. These metrics target the unique challenges of turbid water conditions, focusing on color cast correction and contrast enhancement:

##### Underwater Image Colorfulness Measure (UICM).

This metric quantifies the color quality in underwater images by analyzing the chromatic components in the LAB color space. For an input image  $I$ , we first convert it to the LAB color space and extract the  $a$  and  $b$  channels, which represent the green-red and blue-yellow opponent color pairs, respectively. The UICM is then calculated as:

$$\text{UICM}(I) = -0.0268 \cdot \sqrt{\mu_a^2 + \mu_b^2} + 0.1586 \cdot (\sigma_a + \sigma_b) \quad (36)$$

where  $\mu_a$  and  $\mu_b$  are the means of the  $a$  and  $b$  channels, while  $\sigma_a$  and  $\sigma_b$  are their respective standard deviations. This formulation has two key components: the negative

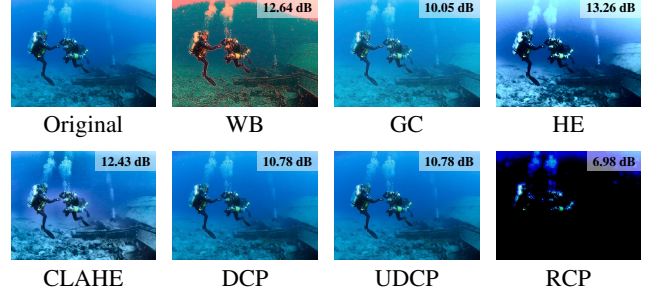


Figure 7. Comparison between traditional UIR methods. Abbreviations: WB - White Balance, GC - Gamma Correction (1.5), HE - Histogram Equalization, CLAHE - Contrast Limited Adaptive Histogram Equalization, DCP - Dark Channel Prior, UDCP - Underwater Dark Channel Prior, RCP - Red Channel Prior.

term penalizes strong color casts (high mean values in either direction), while the positive term rewards color variation and richness (high standard deviations). Higher UICM values indicate better color balance and diversity, which is particularly important for turbid underwater scenes where color distortion is severe.

**Underwater Image Contrast Measure (UIConM).** This metric evaluates local contrast enhancement, which is crucial for visibility in turbid waters. For an image converted to grayscale  $G$ , UIConM analyzes the local standard deviations across the entire image:

$$\text{UIConM}(I) = \frac{1}{HW} \sum_{i=1}^H \sum_{j=1}^W \sigma_{ij} \quad (37)$$

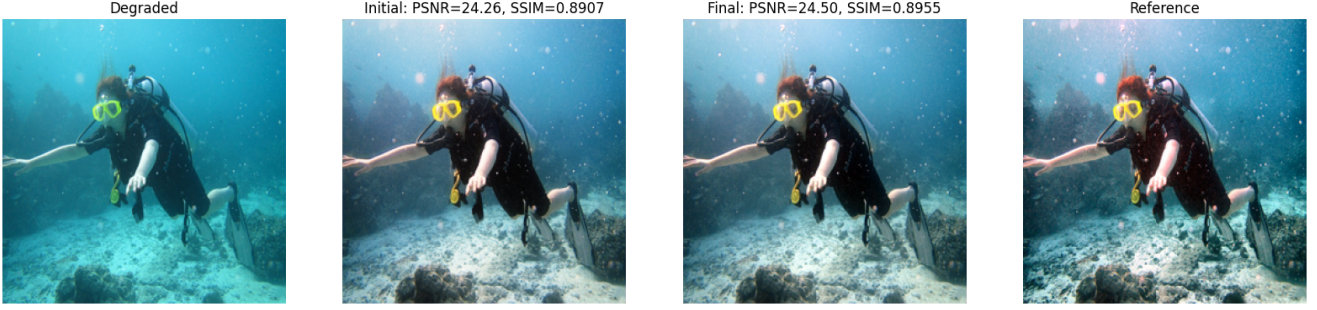
where  $\sigma_{ij}$  is the local standard deviation in a  $5 \times 5$  window centered at pixel position  $(i, j)$ , calculated as:

$$\sigma_{ij} = \sqrt{\frac{1}{N} \sum_{(p,q) \in W_{ij}} (G(p,q) - \mu_{ij})^2} \quad (38)$$

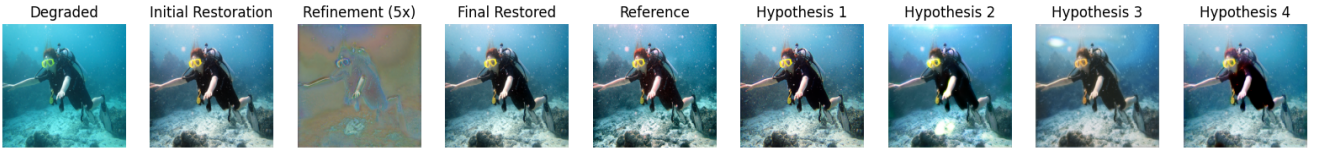
where  $W_{ij}$  is the  $5 \times 5$  window around pixel  $(i, j)$ ,  $N = 25$  is the window size, and  $\mu_{ij}$  is the local mean in the window. Higher UIConM values indicate better local contrast enhancement, which improves visibility of structures and details in turbid underwater environments.

Together, these metrics provide a comprehensive assessment of color correction and contrast enhancement capabilities, which are particularly challenging in turbid water conditions. They complement the standard metrics (PSNR, SSIM, LPIPS) used in our main experiments by specifically targeting the unique challenges of underwater image restoration in turbid environments.

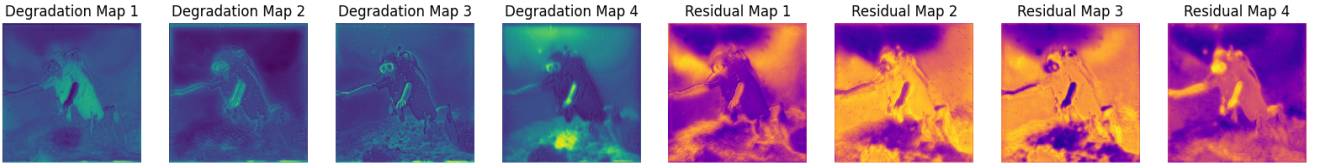
Progressive Improvement: PSNR +0.24dB, SSIM +0.0047



(a) Progressive improvement visualization showing the diver scene. From left to right: degraded input, initial restoration (PSNR=24.26, SSIM=0.8907), final restoration (PSNR=24.50, SSIM=0.8955), and reference image. Our refinement stage achieves a +0.24dB PSNR and +0.0047 SSIM improvement over the initial restoration.



(b) Complete restoration pipeline for the diver scene. From left to right: degraded input, initial restoration, refinement visualization (5 $\times$  amplified for visibility), final restored result, reference image, and the four specialized hypotheses (color, contrast, detail, and denoising).



(c) Degradation and residual maps for the diver scene. Left four images: the estimated degradation maps from the first stage, highlighting color distortion, contrast reduction, detail loss, and noise. Right four images: the residual degradation maps from the second stage, indicating regions requiring additional refinement.

Figure 8. Comprehensive analysis of the diver scene. The degraded image suffers from greenish color cast and reduced contrast. The initial restoration significantly improves color balance, while the refinement stage enhances detail visibility in the diver’s equipment and seafloor textures. The degradation maps clearly identify the upper region as having more severe color distortion, while the residual maps focus refinement efforts on the diver and foreground elements.

### A3. Additional Experiments

#### A3.1. Comparison with Traditional Methods

We compare our TIDE framework against several classical image processing techniques commonly used for underwater image enhancement. As shown in Figure 7, traditional methods exhibit notable limitations. White Balance adjusts RGB channels using the gray-world assumption but fails to account for wavelength-dependent attenuation, leading to unnatural colors. Gamma Correction (1.5) boosts brightness but doesn’t correct color distortion or adapt to local degradation. Histogram Equalization improves global contrast yet often amplifies noise and causes oversaturation, while CLAHE offers better local contrast but still enhances noise and fails to address color casts. Dark Channel Prior, designed for land-based dehazing, performs poorly underwater due to its invalid assumptions in bluish environments.

Its underwater variant accounts for wavelength attenuation but still leaves a bluish tint. The Red Channel Prior enhances the lost red component but tends to overcompensate, resulting in unrealistic reddish tones.

#### A3.2. Extended Hardware Efficiency Analysis

We provide a detailed analysis of TIDE’s computational efficiency to demonstrate its viability for both real-time applications and high-throughput batch processing. Our architecture achieves this efficiency through thoughtful design choices that minimize overhead despite the sophisticated two-stage approach.

Table 3 quantifies the minimal computational burden introduced by our refinement stage. Adding only 1.25M parameters (1.1% overhead), the refinement components generate targeted correction terms rather than full restorations, enabling efficient resource utilization. The runtime memory

Table 3. Hardware efficiency analysis on RTX 4070 Ti SUPER showing the minimal overhead of the refinement stage.

Model Architecture				
Component	Parameters (M)	Size (MB)	Overhead	Memory (GB)
Base Model	114.5	436.9	-	0.44
Refinement Stage	1.25	4.8	1.1%	+0.0
<b>Total Progressive</b>	<b>115.8</b>	<b>441.6</b>	<b>1.1%</b>	<b>0.44</b>

footprint remains unchanged at 0.44GB when adding the refinement stage, demonstrating effective activation reuse between stages. Figure 9 visualizes TIDE’s performance characteristics across different configurations, highlighting three key efficiency mechanisms:

**Parallel Feature Processing.** TIDE’s specialized decoders operate on shared features simultaneously rather than sequentially, enabling efficient hypothesis generation. This parallel architecture yields impressive throughput: at 128×128 resolution with batch size 8, the model achieves 123.4 FPS (8.1ms latency) while maintaining a modest 0.46GB memory footprint. Even at 256×256 resolution, our model delivers real-time performance of 33.4 FPS (30.0ms latency) with batch size 1.

**Selective Computation via Degradation-Guided Fusion.** By applying computation proportionally to degradation severity, TIDE avoids redundant processing in well-preserved regions. This targeted approach enables excellent batch scaling properties: at 128×128 resolution, throughput increases 3× from 40.3 FPS (batch 1) to 123.4 FPS (batch 8) with only a 0.02GB memory increase. Similarly, at 256×256 resolution, the model maintains consistent real-time performance when scaling from batch size 1 (33.4 FPS) to batch size 4 (33.0 FPS) with minimal memory overhead (0.04GB).

**Lightweight Refinement Design.** Our refinement stage achieves efficiency through sparse correction generation rather than full image reprocessing. This approach results in no measurable increase in runtime memory usage while significantly improving restoration quality. The complete performance profile reveals five real-time capable configurations:

- 128×128 (batch 1): 40.3 FPS, 24.8ms latency, 0.439GB memory
- 128×128 (batch 4): 116.8 FPS, 8.6ms latency, 0.44GB memory
- 128×128 (batch 8): 123.4 FPS, 8.1ms latency, 0.46GB memory
- 256×256 (batch 1): 33.4 FPS, 30.0ms latency, 0.44GB memory

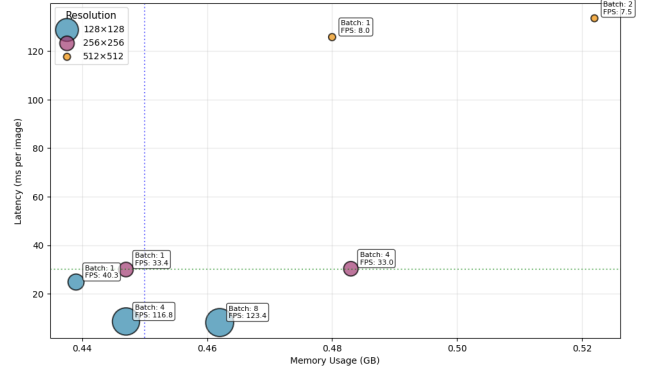


Figure 9. Memory vs. latency analysis across different resolutions and batch sizes. Bubble size corresponds to throughput (FPS). The plot demonstrates TIDE’s scalability and efficiency, with configurations in the lower left quadrant achieving real-time performance (>30 FPS) with minimal memory usage.

- 256×256 (batch 4): 33.0 FPS, 30.3ms latency, 0.48GB memory

For higher resolution applications (512×512), the model maintains consistent throughput of 7.5-8.0 FPS across different batch sizes, suitable for offline processing of high-resolution underwater imagery. These results demonstrate that TIDE’s sophisticated degradation modeling and two-stage approach achieve superior restoration quality without imposing prohibitive computational requirements, making it viable for deployment across a spectrum of hardware configurations and application scenarios.

### A3.3. Extended Qualitative Analysis

To further demonstrate the effectiveness of our two-stage approach, we present additional qualitative results across different datasets. These examples showcase TIDE’s ability to handle diverse underwater degradations and provide a comprehensive view of our restoration pipeline’s internal workings.

These examples provide a comprehensive view of TIDE’s internal workings across diverse underwater scenes. For each example, we present: (1) the progressive improvement from initial to final restoration with quantitative metrics, (2) the complete restoration pipeline including specialized hypotheses, and (3) the degradation and residual maps that guide our restoration process.

In Figure 8, we analyze a diver scene with significant greenish color cast. The progressive improvement visualization shows a +0.24dB PSNR gain from the refinement stage, with noticeable enhancements in the diver’s equipment details and seafloor texture. The hypotheses visualization reveals how different decoders contribute to the restoration: the color decoder effectively corrects the greenish tint, while the contrast and detail decoders enhance visibility of



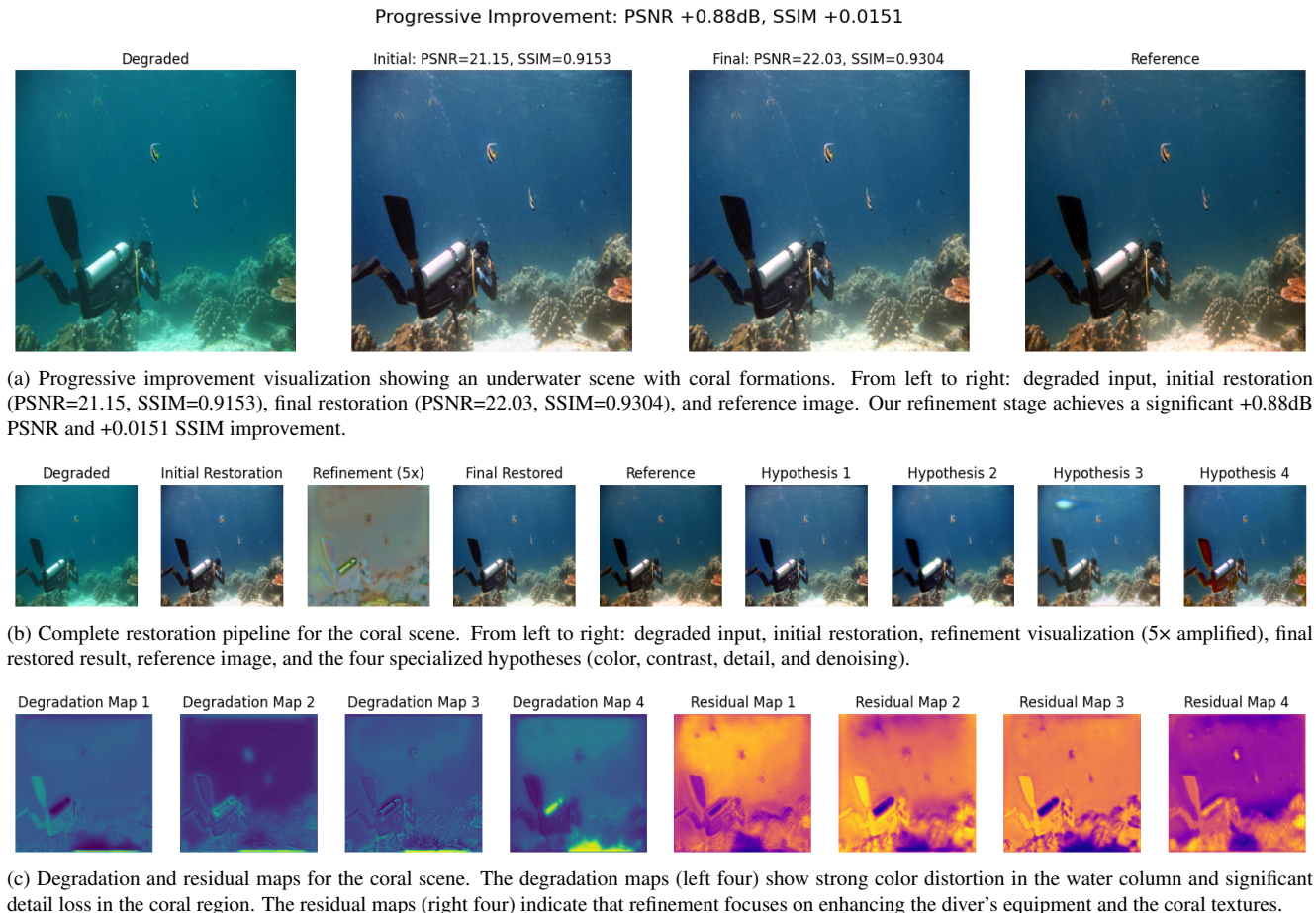


Figure 10. Comprehensive analysis of the coral scene. This example demonstrates TIDE’s ability to handle scenes with complex foreground structures and varying degradation characteristics. The degradation maps indicate stronger color distortion in the water column and noise in the coral regions, while the hypotheses show how each decoder contributes differently to the final restoration.

the diver’s equipment. The degradation maps highlight that color distortion is more severe in the upper region of the image, while the residual maps show that refinement focuses primarily on the diver and foreground elements.

Figure 10 examines a scene with complex coral formations and a diver. This example demonstrates a more substantial refinement improvement of +0.88dB PSNR and +0.0151 SSIM. The hypotheses visualization shows the complementary nature of our specialized decoders: while the color decoder establishes the overall color balance, the detail decoder is crucial for recovering the fine textures in the coral formations. The degradation maps indicate stronger color distortion in the water column and detail loss in the coral region, while the residual maps show targeted refinement in these areas.

Figure 11 showcases the underwater statue example, which exhibits the most significant refinement improvement among our examples (+1.40dB PSNR). The initial restoration successfully corrects the dominant blue-green color

cast, but the refinement stage substantially enhances the statue’s textural details and fine structures. The degradation maps reveal stronger color distortion and detail loss concentrated around the statue, while the hypotheses visualization shows that the color and contrast decoders contribute most significantly to the overall restoration in this case.

These examples collectively highlight several key strengths of our approach. First, the progressive refinement stage consistently improves restoration quality, with PSNR gains ranging from 0.24 dB to 1.40 dB across different cases. Second, the degradation and residual maps reveal the model’s ability to detect and adapt to spatially varying degradation patterns, enabling localized, context-aware adjustments. Third, the specialized decoders produce complementary hypotheses that target different degradation types, which are then effectively fused through adaptive weighting. Finally, the residual maps guide the refinement stage to selectively focus on areas that require further enhancement, while preserving regions that have already been satisfacto-

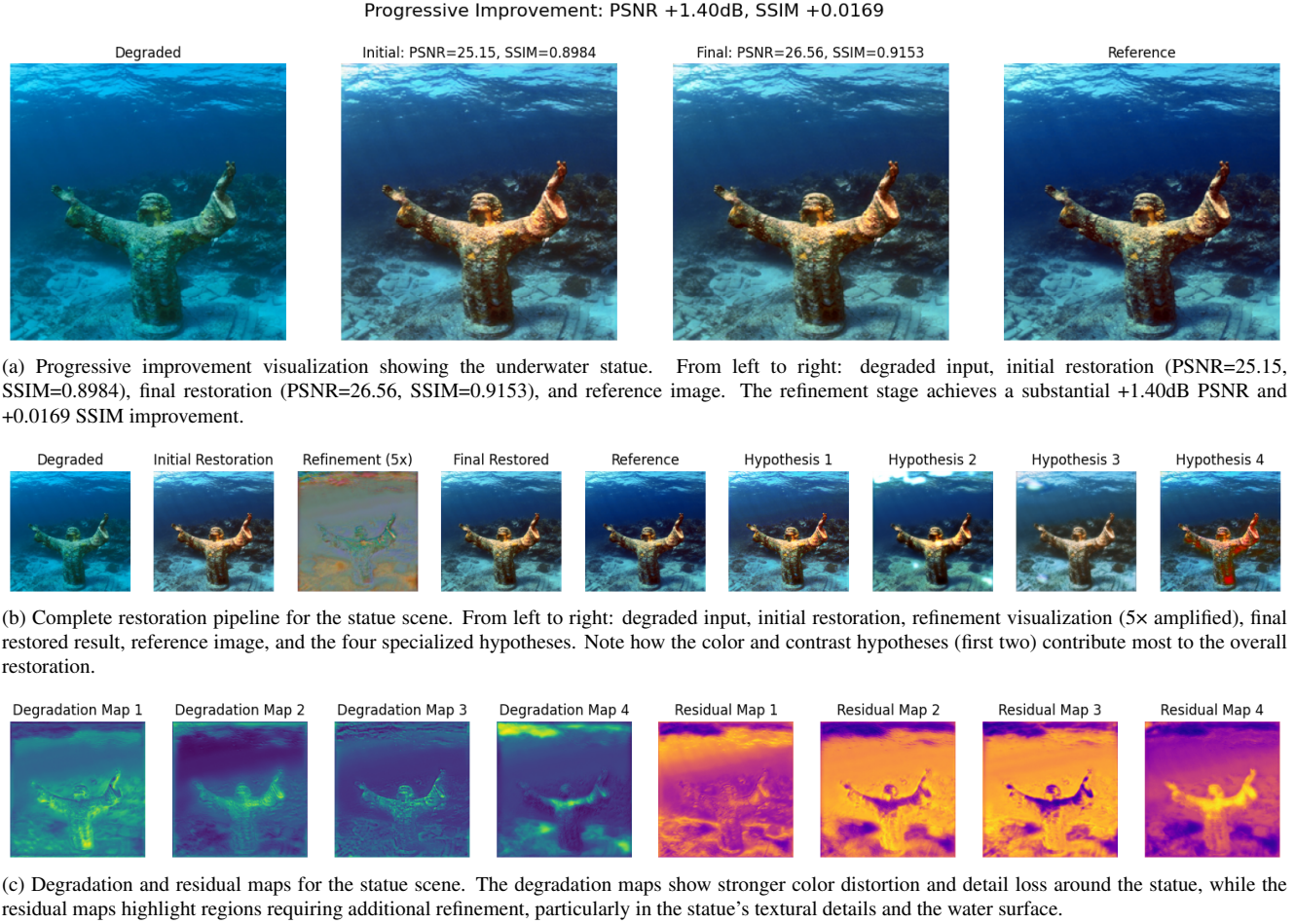


Figure 11. Comprehensive analysis of the underwater statue scene. This example demonstrates the largest quantitative improvement among our examples (+1.40dB PSNR), highlighting the effectiveness of our two-stage approach on challenging scenes with complex structures and non-uniform degradation.

rily restored.

The internal visualizations provided here offer insights into why our approach outperforms existing methods, particularly on challenging scenes with non-uniform degradation characteristics. By explicitly modeling different degradation types and their spatial distribution, TIDE achieves more targeted and effective restoration compared to conventional approaches that apply uniform processing across the entire image.